An Investigation into the Propulsion and Stability Characteristics of the Junk Yacht *Boleh*

Part III Individual Project 2013

M. J. A. Slater

Picture courtesy Boleh Trust, 2013

Project supervised by Professor P. A. Wilson and Dr Z. Chen

"I cannot command winds and weather"

-Horatio Nelson

Abstract

The Junk Yacht *Boleh,* currently undergoing restoration, has been subjected to a series of tests and analyses to help guide renovation work leading up to her re-launch. Under examination were her hydrodynamic resistance characteristics in calm and moderate sea conditions, and her statical stability. A series of towing tank tests and computational fluid dynamics (CFD) simulations were used to analyse the former, while the latter was assessed using computer software. Tank testing and stability assessment aspects were completed successfully, while the CFD element was incomplete at the time of publication. It was concluded that the tank tests predicted the vessel's power requirements significantly lower than reality, that she was stable, and that the CFD model would yield useful results with a limited amount of further work.

Acknowledgements

The author would like to thank the members of the Boleh Trust, Graham Westbrook and Professor Wilson for the help and support they have provided during this project. Further thanks goes to Jonathan Happs, Reshma Rao, Thomas Eldridge and Christopher Fairhall who surrendered their time to assist with the towing tank experiments.

Table of Contents

10004 words.

Nomenclature

Fn	Froude Number
Re	Reynolds number
Ct	Total resistance coefficient
Cr	Residual resistance coefficient
Cf	Frictional resistance coefficient
Cv	Viscous resistance coefficient
Cw	Wave resistance coefficient
Caa	Air resistance coefficient
(1+k)	Form factor
Δ Cf	Hull roughness factor
Y plus	Y+ value
V, u or u8	Forwards velocity of vessel (m/s)
u*	Non-dimensionalized velocity
g	Acceleration due to gravity (m/s^2)
L	Waterline length of Ship or model (m)
v	Kinematic Viscosity (M^/s)
Y	Boundary layer thickness (m)
μ	Dynamic viscosity (Ns/m^2)
ρ	Density (kgm^-3)
p	Pressure (Pa)
GZ	Righting lever (m)
KG	Distance from keel to centre of gravity (m)
CG	Centre of gravity
CB	Centre of buoyancy
GM	Distance from centre of gravity to metacentre (m)

List of Figures

List of Tables

Introduction

The junk yacht *Boleh* is a vessel with a unique and fascinating history. Built in Singapore in 1949, she was sailed by her owner and designer halfway around the world to the south coast of England in an epic eight month voyage (Kilroy R A, 1951). She was then used as a sail training ship for some years, before being sold into private hands (Boleh Trust, 2013). In 2007, she was sold to the Boleh trust to undergo restoration for use as a sail training ship. The restoration process itself is designed to engage local young people and teach shipbuilding and conservation skills (Boleh Trust, 2013).

Boleh's design is as unique as her history; her hull combines elements of historic British yachts and traditional Chinese junks. She also sports a quadruped mast, fully rigged with a mixture of Chinese lug sails and European headsails. She was originally fitted with a novel but temperamental engine design, consisting of a removable “z” drive mounted on her stern (Kilroy R A, 1951). Her particulars can be seen in appendix A1.

As many of the finer details of her rig and mechanical propulsion must be modified or replicated before she can be re-launched, it was decided that some scientific analysis must be performed on her rig, stability and propulsion. The task was divided between the author, who covered the stability and mechanical propulsion aspects, whilst Jonathan Happs investigated her rig in his report “An analysis of the sailing efficiency of the Junk Yacht *Boleh*” (2013). Technical data was provided by Boleh Trust and the naval architect Graham Westbrook.

The most important element in choosing a new engine for a vessel is discovering her hull resistance, and therefore the power required to propel her at each speed. Once this is known, a power-plant of sufficient power can be selected. This project focuses primarily on this, specifically on the naked hull resistance – that is, without appendages such as propeller shafts or rudders. Two methods of investigation were chosen, for the sake of mutual validation – a traditional towing tank test, and a more modern technique, computational fluid dynamics (CFD). Methods involving standard series were not chosen due to the individual nature of Boleh's hull.

Also under investigation was *Boleh's* static stability; safety is paramount on a sail training vessel, and the risk of capsizing must be assessed. An assessment into her stability, using computational methods, was performed as part of the project.

1. Theory of resistance testing using model experiments

1.1 Basis of testing

Towing tank testing is the practice of pulling a scale model of a vessel through a tank of water, in order to determine its hydrodynamic characteristics, specifically its water resistance or drag. The resistance of the vessel is measured using a dynamometer attached to the towing carriage. This carriage is mounted on rails above the tank and towed at a set speed by a system of pulleys. By towing the model at a range of speeds, a curve of resistance versus speed can be produced. This curve can then be scaled to give a prediction of the resistance of the full vessel.

Broadly speaking, there are two main components of hydrodynamic resistance for a ship floating on a free surface; they are frictional and pressure resistance (Tan M, 2011). Frictional resistance is a result of shear forces on the hull, primarily due to the boundary layer, while pressure resistance is a result of the wave making properties of the hull and some viscous effects (Tan M, 2011).

The flow pattern around the vessel can be broken down into two generic components – the wave system and the wake. The wake is a turbulent region abaft the vessel formed from the separation of the boundary layer from the hull, the flow pattern generated by the shape of the hull, and the wave system (Rawson K J and Tupper E C, 1996). The wave system is generated by the pressure forces on the hull, and consist of divergent and transverse wave patterns (Rawson K J and Tupper E C, 1996).

1.2 Scaling model results to full scale

The scaling of the resistance force from the model to the ship is achieved using the non-dimensionalization of the force-based components of resistance, frictional resistance coefficient (Cf) and residual resistance coefficient (Cr). The sum of these components gives the total resistance coefficient (Ct):

$$Ct = Cf + Cr \quad [1]$$

The coefficients Cr and Cf scale to different laws; Cr is based on gravity, so scales using the Froude number "Fn", and Cf on viscosity, using the Reynolds number, defined below (Tan M, 2011). It is not possible on Earth to match both simultaneously, as gravity is constant – without changing viscosity (for the sake of practically), the length of the ship and model would have to be matched (Tan M, 2011). This issue is solved by matching only the Froude numbers, and therefore Cr, of the ship and model. A formula is used, in this case the ITTC57 correlation line formula, to estimate Cf for both, and therefore Ct can be found for the ship.

$$Cf = 0.075/(\mathrm{Log}(Re) - 2)^2 \quad [2]$$

Aside from the formula [1] given above, there are other methods available for determining Ct for the full ship from the model. Equation [1] was derived in the late 19th century by William Froude (Comstock, J P, 1967), and unsurprisingly there have been several attempts since to improve upon it. The resistance components can be broken down into pure wave and viscous parts, Cw and Cv respectively, (Tan M, 2011); and Ct estimated using the formula:

$$Ct = Cv + Cw \quad [3]$$

The complication with this method comes from the calculation of Cv, which relies on Cf and a form factor, k, as can be seen from equation [4] below. The wave resistance component Cw is the same both the ship and the model, in the same fashion as Cr (Tan M, 2011).The form factor allows for the viscous pressure resistance on the hull (Tan M, 2011).

$$Cv = (1+k)Cf \quad [4]$$

Another method to use this form factor is the 1978 ITTC performance prediction method, which attempts to make a more complete summation of the resistance components of a ship. In addition to the wave and frictional components listed above, it is also factors in air resistance, Caa, and the effect of hull roughness, ΔCf (ITTC, 1999). It again makes use of the form factor:

$$Ct = (1+k)Cf(s) + Cr + Caa + \Delta Cf \quad [5]$$

where:

$$Cr = Ct(m) - (1+k)Cf(m) \quad [6]$$

While this method promises greater accuracy with its increased scope, it does require an experimentally derived estimate of form factor, and empirically derived hull roughness and air resistance coefficients (Molland A F, 2002). Form factor (1+k) can be found by assuming that as Fn goes to zero, the wave resistance will become negligible, and as the Ct curve is tangential to the Cv curve at very small Froude numbers (Tan M, 2011):

$$Ct = (1+k)Cf \quad [7]$$

While these formulae can theoretically provide greater accuracy than Froude's original equation, the reliance on empirical estimations and experimentation to find the additional factors and coefficients could potentially lead to a larger number of uncertainties. Therefore for the sake of simplicity Froude's equation was used in this project.

1.3 Considerations

Account must be made of the temperature of the tank and the salinity of water compared to the desired operating conditions, due to effect that temperature and salinity has on the viscosity of water. As temperature increases, viscosity decreases (ITTC, 2006**),** and as viscous resistance is dependent partially on viscosity of the fluid, a correction must be applied to the scaled result to give an estimate of the true value.

As the flow around a real ship is usually turbulent, and the flow around the model laminar at low speeds (based on the Reynolds number, Re), it is necessary to fit studs to “trip” the boundary layer on the model into turbulent flow to produce an accurate representation of the flow on the ship. Recommendations for the size and placement of these studs was given in the ITTC publication “Recommended Procedures and Guidelines, Model Manufacture, Ship Models” (2002).

The issue with the different boundary layers is the difference in flow pattern in the two types of layer. Laminar flows move in smooth layers over the body, while turbulent flows experience random fluctuations in velocity, making the flow extremely complex (Robert, F. et al, 2010). This generates more frictional resistance than laminar flow, (Robert, F, et al 2010) therefore an incorrect flow pattern on the model will give spurious results for the ship. The flow type can be assessed using the Reynolds number [8], as mentioned above:

$$Re = VL/v \ [8]$$

This gives a non-dimensional index of the flow based on length of surface, flow free-stream velocity, and viscosity. Knowing the transition Reynolds number of a plate, it is possible to determine the flow type over the plate (Gemba K, 2007). By approximating the ship as a plate and calculating its Reynolds number, the probable flow type can be found.

At the model scale, it is unusual to include appendages such as bilge keels, fins etc., due to the differences in flow pattern between the model and the full ship, and as such, most model tests are carried out on a “naked” hull. The difference stems from the relative thicknesses of the boundary layers on the ship and model – relative to the hull sizes, the boundary layer on the model can be as much as twice as thick as that found on the ship (Molland A F, 2002). The effect of this is that appendages that may be wholly immersed in the boundary layer on the model may be exposed to the full flow on the ship, and as such, may experience a different drag than predicted (Molland A F, 2002). Therefore, before the powering predictions from the model tests can be used to select an engine, account must be made of these appendages. Further, if the vessel is to be fitted with a propeller, additional tests (self propulsion tests) must be carried out to ascertain the effect of the ship's hull on the flow through the propeller, to find out the efficiency of the propeller and the power required (Comstock, J P, 1967). Finally, account must be made of mechanical losses in the propeller shafting.

2. Theory of static stability

2.1 Principles of static stability

The principles involved in the stability of a vessel are well known and understood, although they are complex to calculate analytically, as they rely mainly on the geometric shape of the vessel under study. The intricate curves found on ships require numerical integration, usually using Simpson's rule, to evaluate sectional areas and volumes – as these areas change with draught, trim, heel etc., it would be too large a task to perform a full stability assessment by hand. Therefore, the hydrostatics software HST, published by the Wolfson Unit at the University of Southampton, was used in the analysis.

The stability of *Boleh* was assessed using GZ curves. The GZ curve, or curve of statical stability, is a plot of a vessel's righting lever, GZ, against its angle of heel. The righting lever is illustrated below in figure 2.1:

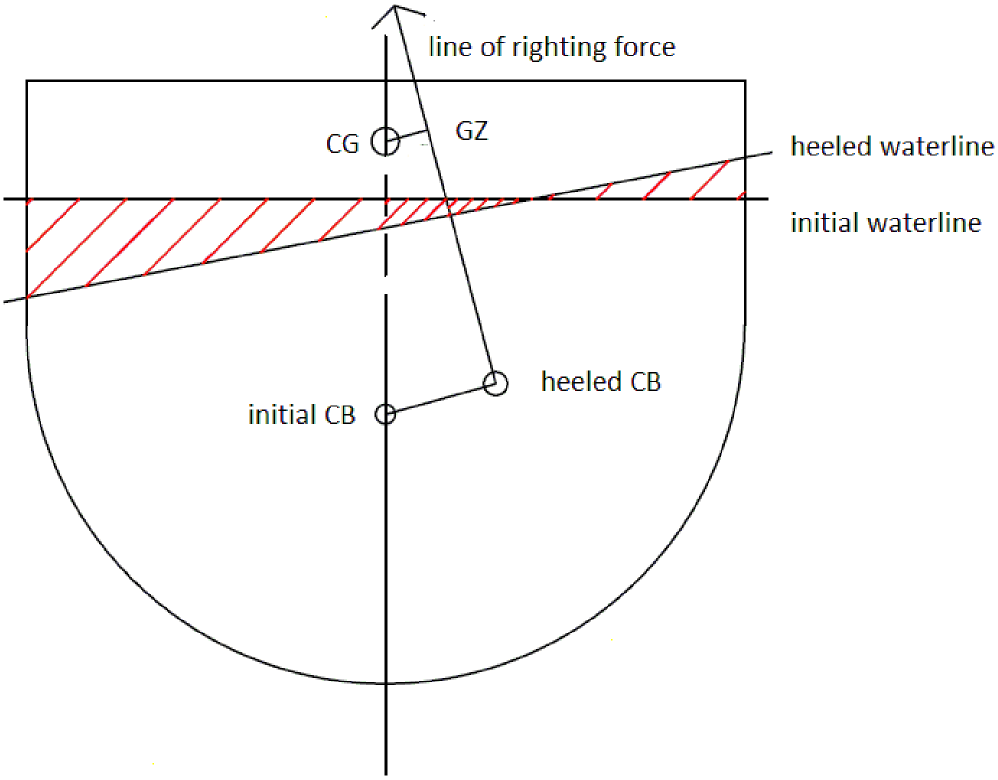

Figure 2.1: static stability of a ship at large angles. Based on a figure from Rawson and Tupper (2001)

Initially, when the vessel is upright, the centre of buoyancy, CB, is in line with the centre of gravity, CG. Therefore, the weight of the vessel, acting through the CG, is line with the upthrust, acting through CB, and the vessel is in equilibrium. When a heeling moment is applied to the vessel, it can be seen from figure 2.1. that the centre of buoyancy will shift as the shape of the immersed area changes. The upthrust will now no longer be acting in line with the weight, and a restoring force is generated. The lever orthogonal to this force, and passing through the centre of gravity, is known as the righting lever, GZ (Rawson K J and Tupper E C, 2001). By plotting this lever against heel angle, the GZ curve is generated.

The height of the centre of gravity above the keel (KG) has a dominant effect on the stability of the vessel. It can be seen from figure 2.1 that increasing KG will reduce GZ, and if increased to too great a height, above the intersection of the upthrust and centrelines, will cause the vessel to become unstable. At small angles of heel this crossing point is known as the metacentre; at larger angles, it moves too much to be considered a fixed point. (Rawson K J and Tupper E C, 2001)

2.2 The free surface effect

It is necessary therefore to include in any stability calculations any phenomena which have an effect on KG. In this case, the relevant issue is the free surface effect:

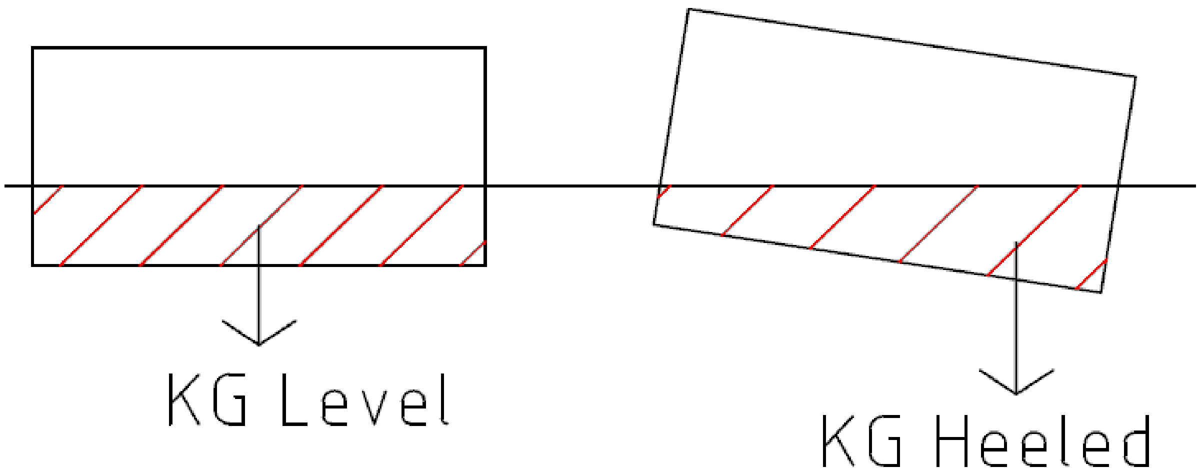

Figure 2.2: the free surface effect

The free surface effect has be visualised in figure 2.2. The hatched area represents the filled volume of the tank; as the vessel heels, the fluid moves to fill one side of the tank, and the centre of gravity shifts with it. As this shift is towards the immersed side, it acts against GZ (Comstock, J P, 1967), and can be modelled as a reduction in KG.

3. Theory of resistance testing using computational fluid dynamics

3.1 Introduction to computational fluid dynamics

Computational fluid dynamics is the numerical modelling of fluid flow around an object. For a laminar flow where the effects of viscosity are ignored, it can be practical to use an analytical hand calculation to derive the forces and moments on an object. For laminar or turbulent flows which factor viscosity, the equations become impossibly complicated to solve, as some (the Navier-Stokes equations), which only describe incompressible flow of constant viscosity, are “coupled, nonlinear, and second order partial differential equations”. They must be solved simultaneously, with no analytical solution having yet been found (Robert, F, Et al, 2010). For this reason a numerical computational method is used. In this case, CFD is being used in parallel with the towing tank testing to find the resistance force on *Boleh.* Due to the complexity inherent in CFD itself, only a steady state analysis of the vessels’ resistance in calm water is being examined, as preliminary research into the effect of added resistance of waves has shown that any such calculation would take an impractical amount of time.

As it is impossible to model the whole domain in which *Boleh* is operating (the ocean), it is necessary to define an arbitrary region of sea round the vessel as a control volume (CV) to approximate the wider ocean (Robert F, et al 2010). The flow is modelled as a steady stream through this volume. At the edges of the control volume, it is necessary to define boundary conditions to ensure that the flow over the vessel is adequately simulated, and that conservation of mass (i.e. the amount of mass entering the system equals the amount leaving it) is observed, in order to achieve steady flow (Robert F,et al 2010).

3.2 The Navier-Stokes equations and finite volume method

The software used in this investigation was Ansys CFX 14.0, a commercial CFD package available at the University of Southampton. In order to solve the flow problem, the program uses a technique called the finite volume method (Versteeg H K and Malalasekera, 1995). The method can be summarised as the conversion of the governing equations into a solvable form within the control volume, which can then be solved iteratively at each point; the equations are converted into a solvable form by a process of integration and discretisation (Versteeg H K and Malalasekera, 1995).

The governing equations for incompressible flows themselves are based on the fundamental principles that the mass of fluid in an incompressible flow flowing into a volume must equal the mass of fluid leaving it, i.e. “the mass of fluid is conserved”; likewise, momentum must be conserved within the fluid volume, as per Newton's second law (Versteeg H K and Malalasekera, 1995). The mathematical relationship that describes the conservation of mass, known as the “continuity of mass equation” (Using CFD) is given as:

$$\frac{\partial u}{\partial x}+\frac{\partial v}{\partial y}=0 \quad [9]$$

While the conservation of momentum equations are given as:

$$\frac{\rho \partial u}{\partial t}+\frac{\rho u \partial u}{\partial t}+\frac{\rho v \partial u}{\partial y}=-(\frac{\partial p}{\partial x})+\frac{\partial}{\partial x}\left(\frac{\mu \partial u}{\partial x}\right)+\frac{\partial}{\partial y}(\mu \frac{\partial u}{\partial y}) \quad [10]$$

The equation [9] is one of three “Navier-Stokes” equations required to describe the momentum of three dimensional flows; the equation given describes the x-direction while the corresponding equations follow a similar pattern and describe the y and z directions. For laminar flows it should be possible to solve these equations exactly (Shaw C T, 1992); however, the problem under examination involves a turbulent flow, and as noted above it is currently impossible to solve these equations for such flows.

This issue is dealt with by splitting the turbulent flow velocity into two components, an average velocity and a fluctuating velocity (Shaw C T, 1992), i.e. the flow is forming random patterns and vortices but is still moving in a net direction. The random component of the flow velocity can be disregarded for the continuity of mass equation [9], as by substituting in the new velocity expression and integrating with respect to time, net velocity becomes zero, generating a time averaged version (Shaw C T, 1992). For the Navier-Stokes equations [10] this is not as simple, as the integrations generate additional terms in the equations; these extra terms are known as “Reynolds stresses” and must be considered in order to accurately model turbulence (Shaw C T, 1992).

3.3 Turbulence modelling and boundary layer definition

A number of different methods are available to model these turbulence terms, generally by simplifying the Reynolds stress terms into more manageable forms. The k-e model used in this project was a “Simple partial differential equation model” (Shaw C T, 1992) based on a set of complex partial differential equations (PDEs), known as “Transport equations” (Versteeg H K and Malalasekera, 1995) which define the turbulent kinetic energy, “k”, within the flow, and its rate of dissipation, “e” (Shaw C T, 1992). A “Boussinesq” relationship (Versteeg H K and Malalasekera, 1995) is used to convert these energies into Reynolds stresses for use in the time averaged Navier-Stokes equations (Versteeg H K and Malalasekera, 1995); therefore by solving the PDEs and using the converted values as the Reynolds stresses in the Navier-Stokes equations the turbulent flow can be solved.

Meshing is the generation within the control volume of a grid of cells and points. These are the discrete points mentioned above at which the governing equations are solved, and as such, a sound mesh is essential for generating an accurate solution. There exists two mesh types, structured and unstructured, the nature of which is straightforward: structured meshes consist of a regular grid of points, while unstructured meshes form an irregular mass of points, in this case arranged around triangular cells (Shaw C T, 1992).

A numerical method, unlike an analytical one, can only solve the problem at discrete points rather than as a continuum (Robert, F, et al, 2010). It is therefore important to ensure that the mesh of points generated around the object under analysis is of sufficient density and bias, and of appropriate structure, to generate accurate results. With a viscous flow, a boundary layer is generated on the surface of the object subject to the flow – as this boundary layer is largely responsible for the viscous forces on the body, a greater density of points is desirable in this region (Anderson, J, 1995). This bias can be determined using the y+ non-dimensional number, which shows “whether the influences in wall-adjacent cells are laminar or turbulent”, (Mohd Ariff et al, 2009**) :**

$$Y \text{ plus} = Yu^*/\mu \quad [11]$$

As the values for y+ are known for each phase of a turbulent or laminar flow, different values of y (layer thickness) can be substituted until the desired y+ value is found. This is important, as each turbulence model is tied to a set range of y+ values, and exceeding the limits for a given model could lead to inaccurate results (Salim S M and Cheah S C, 2009). This can be explained and visualised using figure 3.1 below:

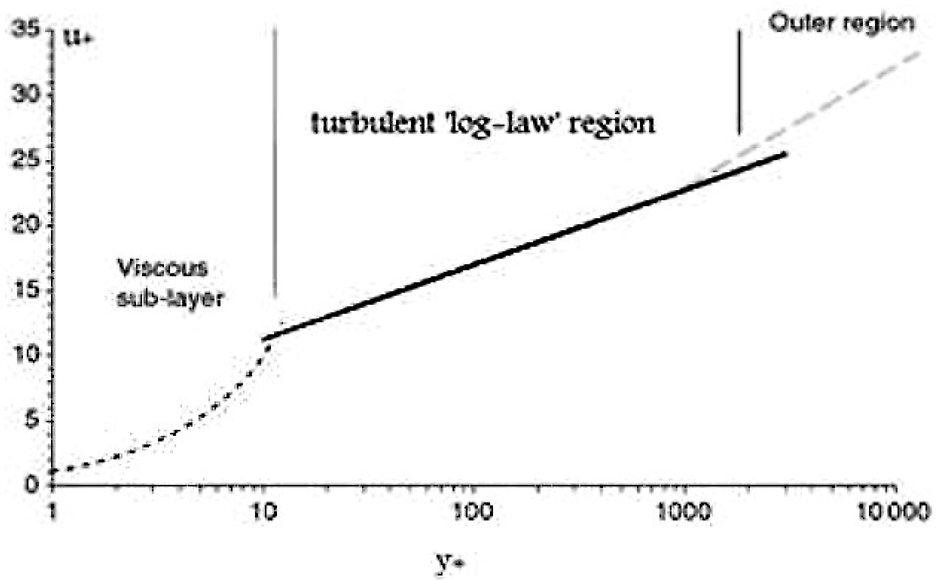

Figure 3.1: From: http://www.flow3d.com/resources/news_10/assessing-mesh-resolution-for-boundary-layer-accuracy.html

Figure 3.1 shows non-dimensional distance from the wall (y+) plotted on a logarithmic scale against non-dimensional velocity (u+). According to Versteeg H K and Malalasekera, (1995) “the shear stress varies slowly with distance from the wall and within this inner region is assumed to be constant and equal to the wall shear stress”; or in other words, a turbulence model operating away from the surface of the body in question may still generate an accurate result by taking advantage of this fact. The k-e model does this, as it operates between y+ values of 30 and 60 (Salim S M and Cheah S C, 2009), giving the advantage that the mesh doesn’t need to be as fine as close to the surface, making mesh generation simpler by lowering the required resolution.

3.4 Simulation in head seas

A full analysis of *Boleh's* performance in a head sea proved impossible to undertake using CFD, as the computation times were extremely high. A paper on added resistance by Gerritsma and Beukelman (1972) provides a possible solution, based on their experimentally confirmed observation that “added resistance in waves varies as the squared wave height”. Although the experiment was conducted on a fast cargo vessel, the analytical equations given in the paper could provide an estimate, with further research, for the wave added resistance on Boleh.

4. Methodology

4.1 Procedure used for towing tank testing

4.1.1 Choice of size and manufacture of model

The first stage involved in the towing tank testing was the choice of a scale, and the construction of a suitable model. In order to select an appropriate scale, a range of model lengths were specified, and the scale speeds for the 2-9 kts speed range required calculated. This gave values for the highest and lowest carriage speeds that would be needed in the tank for a full range of testing, along with a model size and scale. By balancing these three factors a 1/10th scale model was selected. This was on the basis that a model of this scale, approximately 1.2m long, was of a size appropriate for the available tank, had a speed range well within that possible in the tank, and was convenient for scaling linear dimensions such as length, breadth or trim. Table 4.1 below illustrates the selection method.

Scale	Model LWL (m)	Scale speed @ 1kts full size (m/s)	Scale speed @ 9ktsfull size (m/s)
4.75%	0.5	0.22	1.01
5.70%	0.6	0.12	1.10
6.65%	0.7	0.13	1.19
7.60%	0.8	0.14	1.28
8.54%	0.9	0.15	1.35
9.49%	1	0.16	1.43
10.44%	1.1	0.17	1.50
11.39%	1.2	0.17	1.56
12.34%	1.3	0.18	1.63
13.29%	1.4	0.19	1.69
14.24%	1.5	0.19	1.75

Table 4.1: potential model sizes

Once a model size had been decided upon, the digital model of *Boleh* provided by the naval architect responsible for the restoration, Graham Westbrook (Private communication, 2012), was modified and given to the Engineering Department Manufacturing Centre (EDMC) at the University of Southampton. This computer model was then used to construct a fibreglass model of the vessel for use in the tank.

4.1.2 Derivation of testing matrix

The towing tank tests conducted on *Boleh* were based on determining her naked hull resistance in calm water and in the operating conditions she would be likely to encounter in service. The expected conditions were determined based on the vessel's category within the MGN280 code – class 2, and on the conditions in her likely operating areas, the Solent and the English Channel (Westbrook G, Private Communication, 2012). With these conditions in mind and the model ordered, a testing matrix (Table 4.2) was built up for use in the Lamont tank at the University of Southampton. The range of speeds to be tested were chosen based on the likely maximum speed of the vessel – given as 7kts by the Boleh Trust. The highest speed to be tested was set at 9kts, in order to generate a fair resistance/speed curve for the vessel.

Testing was carried out for two different sea states – a calm water condition and a simulated regular head sea equivalent to the most likely operating condition. Only regular seas could be simulated due to the equipment available. Additionally, for each sea state, testing was run for even trim, trim forward and trim aft conditions. This was done because changes in trim result in a change in waterline length, which in turn will change the wetted area and profile of the craft – affecting both frictional and pressure resistance. The vessel was ballasted in the tank to a point scaled from her design waterline in the loaded condition.

The relevant wave lengths and heights were initially derived from data found in "Global Wave Statistics" (Hogben N et al, 1986). In the planning stage it was intended that three sea conditions would be tested, a calm water condition as a control, a likely moderate sea condition to give an indication of the most likely resistance in service, and a rough condition to ensure the vessel would have enough power to return to a safe haven in the event of being caught in a storm. However, it was soon discovered that the equipment in the tank was not capable of producing waves of sufficient magnitude to simulate the chosen conditions; instead the same wavelength was used with the greatest practicable wave height, which was found to be 8cm, with an associated period of 0.55 seconds.

Full Ship Speed(Kts)	Tank Carriage Speed (m/s)	Calm	Calm	Calm	Moderate	Moderate
2	0.325	0m	0.01m aft	0.01m fr'd	0m	0.01m aft
3	0.487	0m	0.01m aft	0.01m fr'd	0m	0.01m aft
4	0.649	0m	0.01m aft	0.01m fr'd	0m	0.01m aft
5	0.811	0m	0.01m aft	0.01m fr'd	0m	0.01m aft
6	0.974	0m	0.01m aft	0.01m fr'd	0m	0.01m aft
7	1.136	0m	0.01m aft	0.01m fr'd	0m	0.01m aft
8	1.298	0m	0.01m aft	0.01m fr'd	0m	0.01m aft
9	1.461	0m	0.01m aft	0.01m fr'd	0m	0.01m aft

Table 4.2: towing tank testing matrix

4.1.3 Configuration and calibration of the model in the tank

Testing in the Lamont tank was carried out with the aid of an assistant. The model was connected to the carriage by means of a towing post, the top of which was connected to the dynamometer and the bottom to a wooden plate installed at the intersection of the waterline and longitudinal centre of flotation, the point about which the vessel trims (Rawson, K.J. and Tupper, E.C.,2001). The fitting at the bottom of the post was only capable of moving freely in one direction; as the vessel was being tested in head seas, she was left free to pitch. The arrangement is illustrated below in figure 4.1.

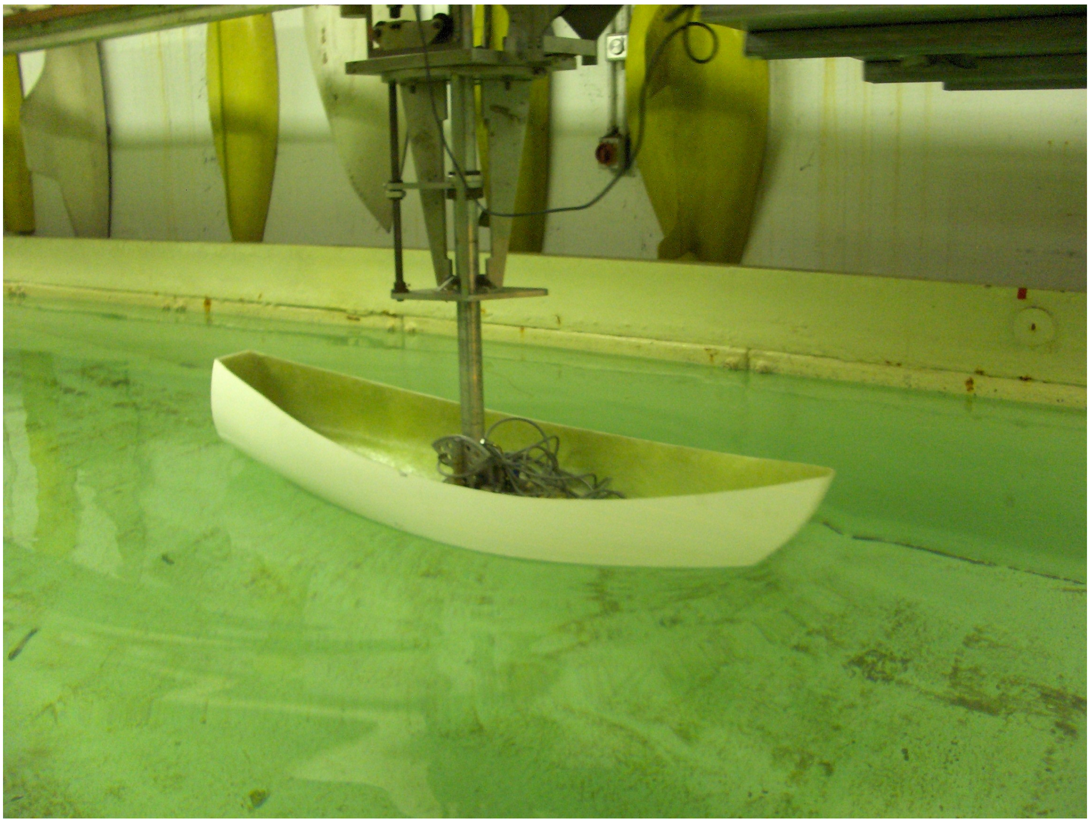

Figure 4.1: the arrangement of the model on the towing post.

The signal from the dynamometer was in the form of a voltage, which was recorded on a computer. By calibrating the equipment with known weights it was possible to achieve a conversion between the voltage and force and derive the resistance force on the model. This calibration was performed twice for every day of testing to help ensure accuracy.

One issue with the experimental arrangement was the location of the towing post fitting in the model. It has been mentioned that it was fitted at the LCF, in order to allow the model to trim correctly; however this did mean that when the vessel pitched in the simulated head sea, it was forced to do so at a point removed from the natural centre of pitch, which was assumed to be through the centre of gravity (Rawson, K.J. and Tupper, E.C.,1996). Further, it was not possible to replicate the exact distribution of mass aboard the model *Boleh.* The available masses used for ballast could only be fitted loose in the bottom of the model. This meant that the radii of gyration were not evenly scaled between the model and boat , and that the vessel would respond to waves with a marginally different pitching period (Rawson, K.J. and Tupper, E.C.,1996). It was decided however that as the major masses in the boat, such as the tanks and engine, were located in approximately the same place as the weights the model, the difference was acceptable and that the error should be small.

4.2 Method of stability assessment

4.2.1 Assessment criteria

The stability assessment for Boleh was carried out according to the guidelines set out in the MGN 280 code. The MGN 280 code does not actually specify any stability criteria for *Boleh*, other than an inclining experiment upon her re-launch, as her intended operating range places her inside Area Category 2 (up to 60 miles from a safe haven) (MCA, 2004). However, for the purposes of this study, the optional criteria applicable to Area Categories 0 and 1 have been used to assess her stability. Unlike the CFD and towing tank tests, the stability assessment was carried out with a full scale model of *Boleh*.

The criteria dictate that for the two load cases, 10% laden and 100% laden (hereafter referred to as arrival and departure respectively), principally, the vessel's GZ curve “should have a positive range of not less than the angle determined by the formula in the table in section 11.9.5, or 90 degrees, whichever is the greater”, and “in addition....... the angle of steady heel obtained from the intersection of a 'derived wind heeling lever’ curve with the GZ curves referred to in section 11.8.1 above should be greater than 15 degrees” (MCA, 2004). The wind heeling lever is simply the distance from the centre of lateral resistance to the centroid of the sails (Fossati, 2009). A mathematically derived version calculated from a formula in the code is used in this case.

4.2.2 Generation of digital model

As mentioned above, the Wolfson unit's HST software was used in the assessment. The same computer model used in the CFD and for the towing tank model was used for the sake of consistency. A modification was made within HST – the model was divided into buoyant and floodable sections, as the overhanging stern of Boleh is open to the elements at the back, abaft a watertight transom.

4.2.3 Estimation of the free surface effect

The free surface effect presented the greatest issue in the stability assessment as the exact shapes of the tanks were not known, and the tanks on either side of the vessel were not of the same shape or capacity. This made it very difficult to program them directly into HST, which could normally have directly calculated the effect on GM at each heel angle. For this reason, an alternative method of determining the effect of the free surface was used. It has been noted that the free surface effect can be regarded as an increase in height of KG; as KG was already programmed into HST, an estimate of the effect was calculated by finding the reduction in GM caused by the tanks and adding the difference to the KG value.

This method will only hold true for relatively small angles of heel, as GM shifts noticeably at larger heel angles. This was not ideal, as some the assessment criteria apply up to and around 90 degrees (MCA, 2004).

The KG values and tank capacities used were derived from data supplied by Graham Westbrook (Private Communication, 2012). These were combined with a general arrangement (GA) from the same source showing the tank locations and some of their dimensions. The KG value for the 10% loaded condition was found by assuming these tanks were square in section and performing a moment balance; likewise, the change in KG due to the free surface effect was found using the second moment of area of the fluid within these tanks at rest. The free surface effect was modelled for both load conditions, despite the lack of free surfaces in the fully laden condition. This was specified in the MGN280 code (MCA, 2004). By assuming the tanks were square, an estimate of the effect of the free surface was again found; the effect is dependent on the second moment of area of the fluid within the tanks, which itself is dependent on the square of the width of the tank (Calvert, J R and Fararr, 2008). As square tanks are wider at the bottom than a tank fitted to the inward curve of a ships hull, the second moment of area must be greater and therefore represents a worst case scenario.

With the relevant values calculated, the simulation was run for each load case and the results, in the form of GZ at each heel angle, plotted.

4.3 Application of computational fluid dynamics to resistance testing

4.3.1 Background and procedure

The CFD component of the project proved to the the most technically complicated of the three elements completed. For this reason, the first few months of the project were taken up with building simple simulations to test concepts and build understanding.

Once a sufficient amount of preparatory work and research had been completed, work started on building a model for the simulation. This can be broken down into three stages:

- Construction of a 3D model
- Meshing
- Flow definition

Different software packages were used for each stage; Maxsurf and Solidworks were used to construct the 3D model, meshing was performed in ICEM and flow definition in ANSYS CFX pre-processor.

The first stage, construction of a 3D model, was relatively straightforward. The same digital model used in the other two studies was used; a rectangular control volume was built around the vessel to contain the fluid and the whole system scaled to 1/10th scale to be at the same scale as the towing tank test. The size of the control volume was based on the width and depth of the Lamont towing tank, with allowances fore and aft equal to approximately 3 and 5 model ship lengths respectively.

The control volume was chosen to be this size for three reasons: The width and depth were chosen to match the tank dimensions so that the final results would match those from the towing tank tests, for the purpose of validation. The allowances fore and aft were chosen so that the significant parts of the wake and wave system would be captured, and so that the flow did not reverse at the inlets and outlets - an issue that plagued earlier tests with smaller control volumes and often led to non-convergence. The final reason was for practicality – by testing at model scale, a denser mesh for the same number elements could be used, requiring less computing power and improving accuracy.

4.3.2 Mesh generation

Of the two mesh types available, a structured mesh could theoretically generate a solution in a shorter amount of time than an unstructured mesh (Shaw C T, 1992) but would be harder to generate for the complicated shape of *Boleh*'s hull. For this reason, an unstructured mesh was used. In order to capture the detail of the boundary layer, a “prism”, a semi-structured area of mesh, was used in the region of fluid adjacent to the hull. This prism allowed fine control of the “y” value, the width of the first cells adjacent to the hull, to be defined with accuracy. Ensuring that the “y” value was correct for each flow speed was essential, since the “k-e” turbulence model required a “y+” value – which was dependent on “y” - within a set range to function properly.

It was stated previously in equation [11] that “y+” is dependent on cell height “y”, dynamic viscosity “μ ” and a value “u*”. This value “u*” is a non-dimensionalised velocity based on the Reynolds number of the vessel; to estimate its value in order to find the requisite “y” at each flow velocity, an empirical relationship was used (Xie Z, 2012):

$$\frac{u^*}{(u8)^2} = 0.0296(Re)^{-0.2} \quad [12]$$

his relationship [12] is based on a “power law approximation for turbulent boundary layers” (Wilson P A, 2012). It gives an approximate value of “u*” for flow of the same speed over a plate of the same length; this estimate provides a “first guess” for the height “y”. See table 4.3:

Flow Speed u8 (m/s)	(u*/u8)^2	u*	y (m)
0.3	2.43E-03	1.48E-02	2.70E-03
0.5	2.19E-03	2.34E-02	1.70E-03
0.7	2.05E-03	3.17E-02	1.26E-03
0.8	1.99E-03	3.57E-02	1.12E-03
1	1.91E-03	4.37E-02	9.12E-04
1.1	1.87E-03	4.76E-02	8.37E-04
1.3	1.81E-03	5.53E-02	7.21E-04
1.5	1.76E-03	6.29E-02	6.33E-04

Table 4.3: cell height (y) for each flow speed

Outside of the prism, the mesh was left as a single continuous zone within the control volume. Some thought was given in regards to including a denser region of mesh aft of *Boleh* to capture an increased amount of detail in the wake. As the overall control volume size is relatively small, and there is a limit on the maximum number of cells that can be used, it was decided that a denser area would not be used.

4.3.3 Boundary conditions

With the mesh generated, the pre-processor part of the Ansys CFX package was used to program the boundary conditions, initial conditions and general details of the flow. Unlike many CFD applications which require only a single phase, the presence of a free surface necessitated a multiphase flow. Due to this and the huge range of options available in CFD software, the set-up was based on a tutorial.

The most important element of the set-up was the definition of the boundary conditions, illustrated in figure 4.2. In practical terms, these define the flow velocity, its pressure, where it enters the control volume and where it exits. An inlet was defined forward of Boleh while the outlet was set as an opening immediately aft. An opening rather than a true outlet was used in case the flow was reversed (i.e. eddying) due to the wake at that point. Experience showed that this could lead to a failure to converge. The roof was also defined as an opening to simulate the open top of the tank. The walls of the tank, and the hull of *Boleh* were defined as walls. The tank walls were defined with a free slip condition, i.e. free from a boundary layer, to simulate the boat moving rather than the fluid. *Boleh* on the other hand was defined with a non-slip condition to allow a boundary layer to form.

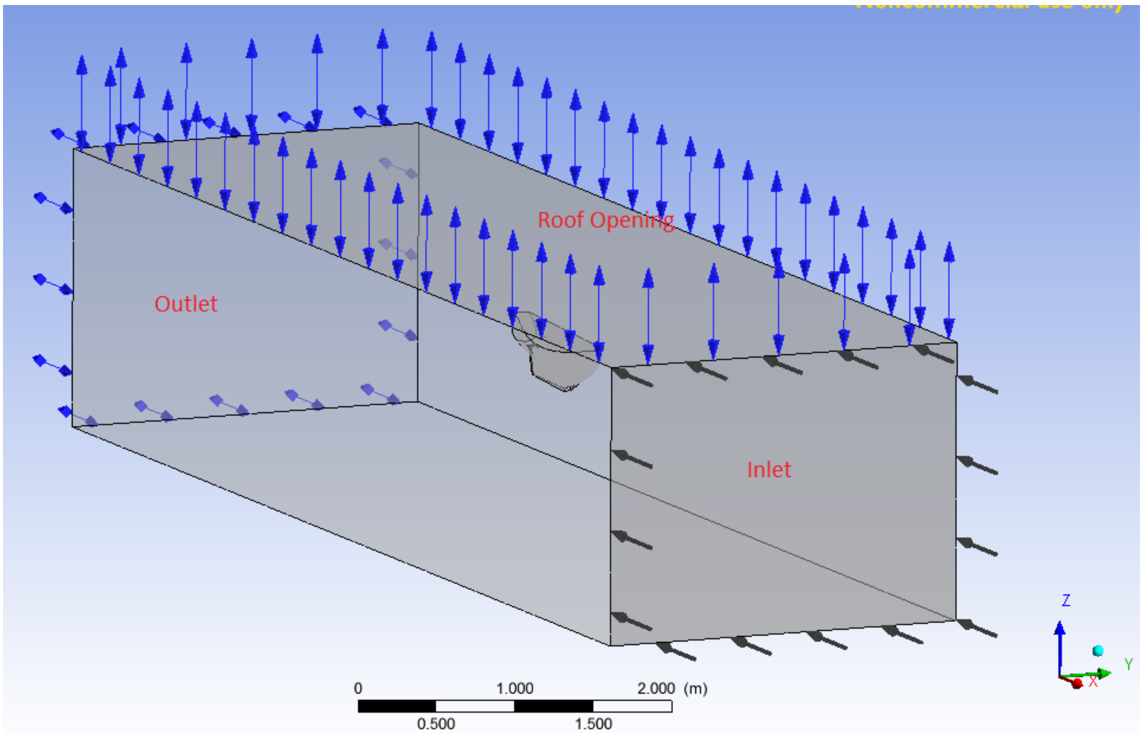

Figure 4.2: illustration of selected boundary conditions.

The multiphase flow necessary to simulate the free surface was programmed using a combination of conditions. A short list of simple code expressions in the CEL code language, derived from the bump tutorial (Ansys, 2010), was entered into the software to control the volume ratios of the air and water phases entering the control volume. It was in the manipulation of variables in these expressions that the correct water height in the tank/draught was defined. Buoyancy and gravity forces were then specified, which put the phases in the correct order. Finally, the initial conditions were set so that the volume was full of water from the outset.

4.3.4 Solution method

The final stage before testing began was inputting the solution method. A range of schemes and precisions are available in CFX that have varying effects on the result. In this case a “High Order”, “Upwind” solution method was chosen. Upwind refers to the order of the solution; in this instance, the velocity solution of each cell upwind of the cell under examination is used to help that cell converge (Shaw C T, 1992).

CFX solver was used to execute the solution. Each run was to be set for a particular flow velocity. As CFD is a numerical method, a number of iterations are performed until the residual error from the exact solution is below an acceptable value. Convergence in this sense refers to this reduction in error; once a solution has reached the required accuracy it is said to have converged (Shaw C T, 1992).

4.3.5 Mesh dependency analysis

Before testing could begin in earnest, it was necessary to perform a mesh dependency analysis. One definition of convergence in the context of CFD has been noted above; another is given as “the property of a numerical method to produce a solution which approaches the exact solution as the grid spacing, control volume size or element is reduced to zero” (Versteeg H K and Malalasekera, 1995). In other words, in order to precisely replicate the flow conditions within the control volume, it would be necessary to make the control volume infinitely small or infinitely finely packed with cells – this is logical as the real flow is a continuum rather than a collection of discrete points. Clearly, a mesh with any infinite properties would require an infinite amount of time to process; the compromise is to measure a single quantity within the simulation, such as the force on *Boleh,* for a single flow speed while reducing the mesh size. When the force becomes more or less constant for each run a mesh of appropriate density has been found. This was not achieved, however, due to time constraints. It was not possible to run the final calculations. In order to ensure accuracy the mesh dependency would have needed to have been repeated for every flow velocity, as the mesh changes in detail due to the shifting values of "y" at each speed.

5. Results and Discussion

5.1 Towing tank tests

Towing tank testing was carried out on six separate days, over the course of several months. It was decided not to split runs between different days, as the cold weather over the winter caused the temperature of the tank to drop steadily through the testing period. Testing in this fashion ensured that for each set of runs, the viscosity of the water was constant, reducing the possibility of errors from additional correcting calculations. Testing was carried out for trim forward, aft and even conditions for the calm water tests, and aft and even for the the moderate conditions.

Time constraints meant that the trim forward test could not be completed for the moderate condition. Where possible, runs were repeated in order to validate the results already gathered; typically, three runs were repeated per set of runs.

The voltage from the dynamometer was not constant, due to myriad factors that will be examined later; therefore an average had to be taken to give a single figure for the resistance force at each speed. The mean was taken from the "steady state" part of the run – i.e. the acceleration and deceleration phases were not included in the average.

5.1.1 Temperature Correction

Once gathered, the results were processed and subjected to a temperature and salinity correction in order to standardise them. The properties of water at the temperature of the tank were used first to determine the resistance of the full scale ship at that temperature. These properties were taken from an International

Towing Tank Commission (ITTC) guidelines (International Towing Tank Conference, 2006). A correction was then applied using the frictional coefficients of the full ship in freshwater at the actual tank temperature, and a frictional coefficient for the vessel in seawater at 15 degrees Celsius; the method was taken from (Tan M, 2011). The formula used, from the same source, was:

$$Ct(15) = Ct(T) + (Cf(15)-Cf(T)) \quad [13]$$

5.1.2 Presentation of select data

The final results for the naked hull power estimate are presented here. The data has been presented in the form of speed/power curves, in order to illustrate the changes in powering requirements with trim and sea state. The curves themselves are included only to make the trends more visible.

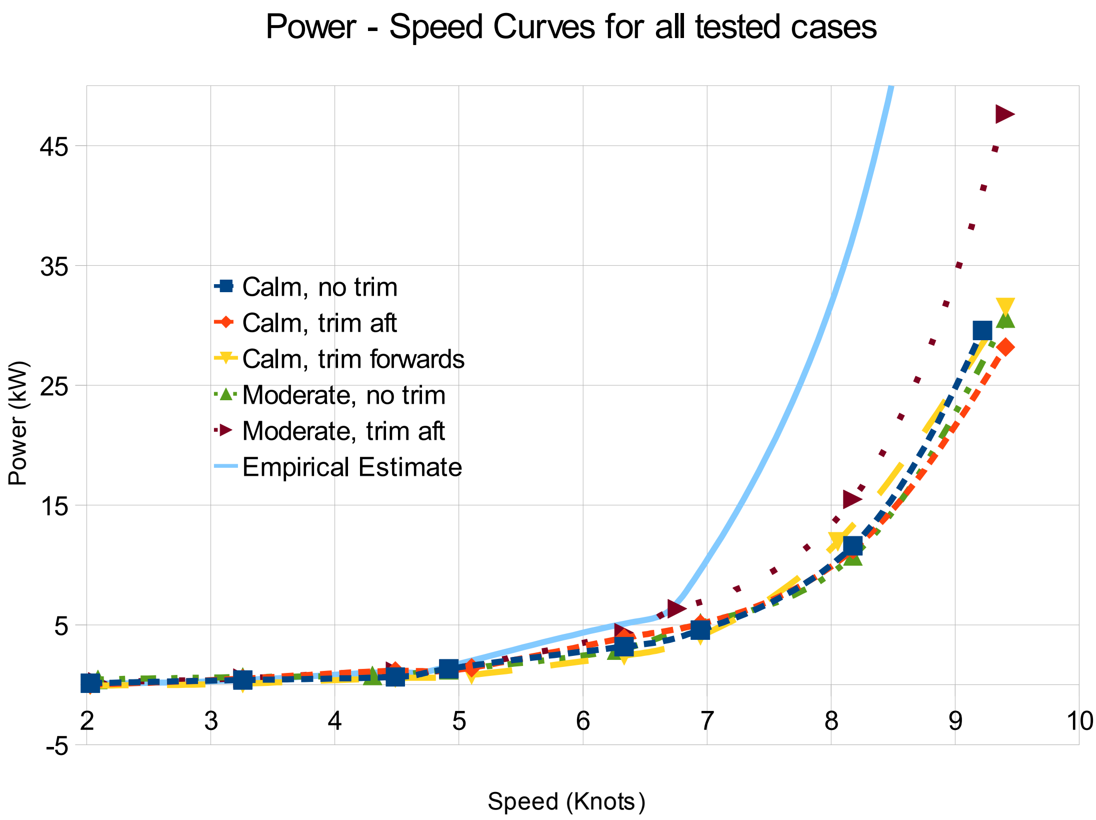

Figure 5.1: speed power curves

The graph 5.1 shows that broadly speaking, trim and sea state has little effect on the powering requirements at low speeds, but the differences become more pronounced as speed increases beyond 5 knots. The curves follow the expected pattern, with power trending towards infinity as hull speed is reached. Even at the higher speeds, the grouping of points is quite tight, excepting the moderate trim aft condition. On the whole, the curves are smooth, although small humps are present for the calm, no trim, and moderate, trim aft curves. One interesting feature of note is that for some cases, the power requirement is negative at very low speeds; a result of experimental error.

The results give rather low power requirements for the vessel; without results from the CFD, another method of validation was required. A paper by J Holtrop and G.G.J. Mennen (1982) provides a method to find an approximate power requirement. This used empirical equations, derived from model tests and full ship data (Holtrop and Mennen,1982). The equations predicted directly the frictional and wave resistances and made an allowance for hull roughness. The results can be seen plotted alongside experimental data in figure 5.1 above. They provide a good match up to 5 knots, a reasonable match up to ~6.8 knots, and are wildly inaccurate above this figure. Full numerical results are presented in appendix A2.

5.1.3 Discussion of data and observations

In terms of trim in the calm water cases, the reason for the grouping is fairly straightforward; the change in waterline length upon which Cf is partly based is only 5mm for the trim cases specified. It is harder to explain why the moderate, trim aft case has a power requirement so much higher than the others at higher speeds, and why the moderate no trim case does not. A possible explanation for the difference present in power between the calm and trimmed cases is that the change in trim shifted buoyancy forwards, increasing interaction with the oncoming waves. This would have generated a greater pitching motion on the vessel, stealing momentum and pushing power requirements up. However, given that the change in trim is small, and that it would be expected for power requirements to increase generally in a head sea anyway, it seems more likely that the curve for the moderate, no trim case suffered from the temperamental performance of the wavemaker on the day of testing.

The general minor variations in the shapes of the curves, such as the occasional bumps and differing gradients, may be put down to error, or to the effect of the wave system. The interaction of the waves generated by the vessel may be constructive or destructive, and could account for the variations in power required at each speed and trim as the waves move in and out of phase. There are no major humps however which would be indicative of severe interference. An example of the wave system generated can be seen in figure 5.2 below; the divergent waves and transverse waves can clearly be seen.

Figure 5.2: wave system in the towing tank. The apparent forward trim is an optical illusion generated by the bow wave.

The empirical estimate provides reasonable validation for the results up to 5 knots, but predicts higher values above this. The difference is down to the statistical nature of the estimate; the vessels used in the regression which generated the equations were highly unlikely to be shaped like *Boleh,* and therefore once wave resistance became dominant at higher speeds, the results became inaccurate.

5.1.4 Error analysis

The error present in the experiment is mainly due to the equipment used; the environment is damp in the towing tank, and there is rust present on the carriage rails. This undoubtedly caused some of the vibrations responsible for the oscillating voltage recorded by the dynamometer. The vessel was observed to pitch during the calm water tests, likely causing further oscillations in the voltage. Ripples on the surface and underwater currents would have caused the remainder -although the tank was left for 10 minutes between runs to settle, small disturbances would still have been present. The wave making machinery proved temperamental, especially for the first run in moderate sea conditions – it was very difficult at times to reliably generate a set of waves of the correct magnitude. Further, the wave heights had to be measured with a simple ruler, leading to minor variations in wave height between runs.

The error causing the power requirements to be negative in the calm, trim forwards case either results from the ITTC formula predicting the frictional resistance coefficient higher than it should be at this speed, or from a slightly anomalous run – large vibrations could lower the average measured drag, resulting in a total resistance coefficient lower than the actual value.

5.2 Stability Assessment Results

Once the software had been set up, *Boleh*'s stability was assessed for the 100% and 10% load cases required by the MGN280 code (MCA, 2004). Free surface effects were included in the calculations for both cases, as specified in the code. The GZ curves generated can be seen below:

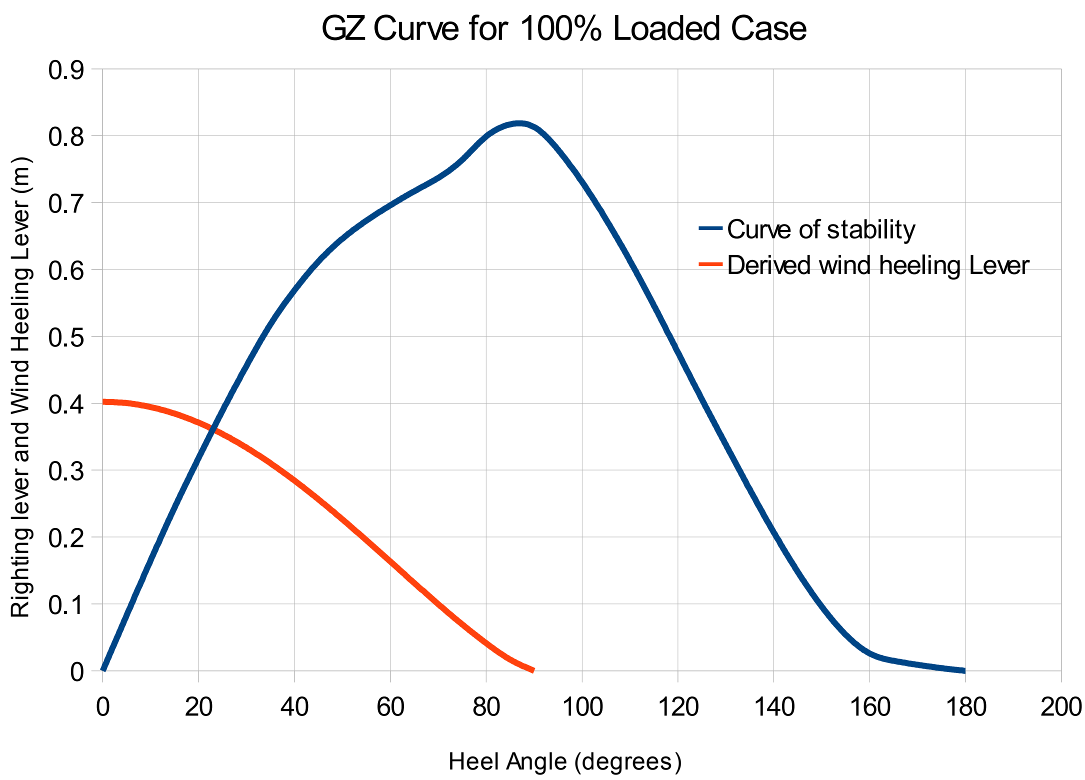

Figure 5.3: GZ curve for fully laden condition.

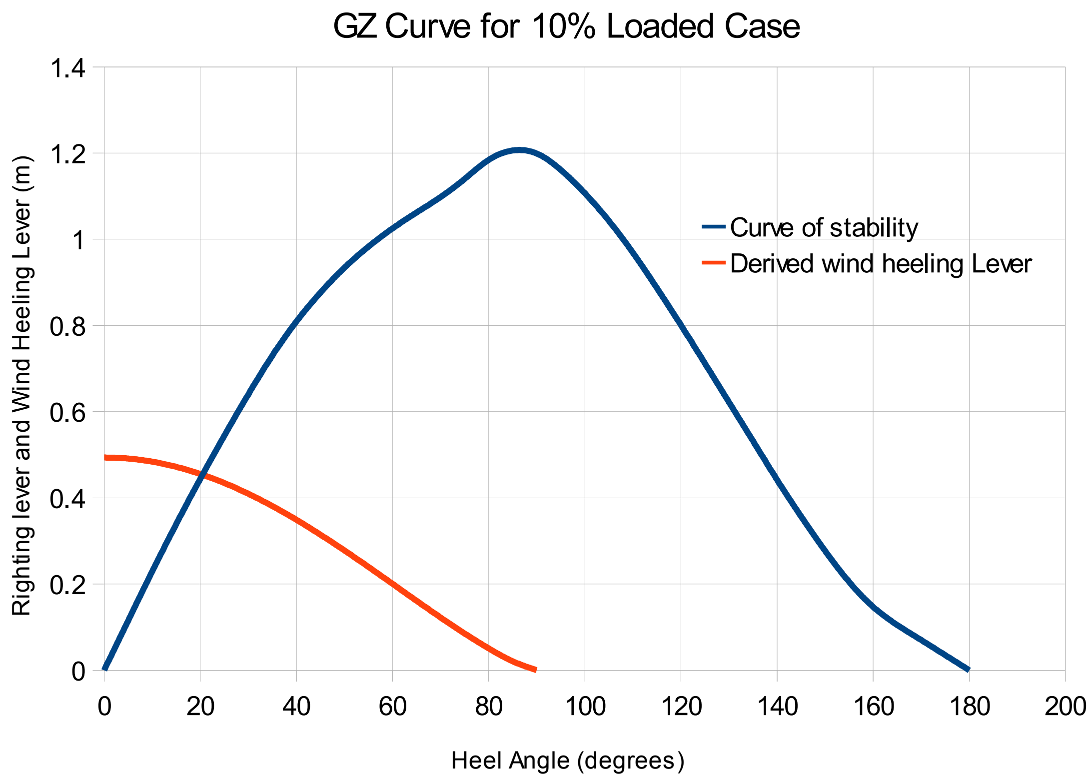

Figure 5.4: GZ curve for partially laden condition.

Both figures 5.3 and 5.4 fit the pattern expected, with stability increasing to a maximum then falling to nothing. The vessel is very stable, with positive stability all the way to 180 degrees (although in practice sails and rigging may diminish this stability if underwater). The wind heeling lever follows a similar curve to that demonstrated in the MGN280 code (MCA, 2004), as it starts at a high value and decreases as the centre of pressure on the sails nears the water due to the heeling action.

The maximum values of the righting lever GZ differ between the load cases, with the 10% load case having the slightly higher maximum GZ. This can be explained by the difference in vertical centre of gravity between the two cases – in the 10% load case, the near empty tanks result in a lower KG value than the 100% loaded case, and therefore a greater righting lever.

5.2.1 Assessment with respect to specified criteria

Boleh easily met all of the criteria specified in the code, which were specifically:

- "The GZ curves required by Section 11.8.1 should have a positive range of not less than the angle determined by the formula in the table in Section 11.9.5, or 90°, whichever is the greater."
- "In addition to the requirements of Section 11.8.2, the angle of steady heel obtained from the intersection of a "derived wind heeling lever" curve with the GZ curves referred to in Section 11.8.1 above should be greater than 15 degrees (see Figure 11.1)."

-(MCA, 2004)

A quick visual check of the GZ curves confirms the first point – the vessel is stable to 180 degrees in both cases, which is the maximum it can be. Of course in reality, flooding would occur long before this angle is reached, as hatches would begin to be immersed at around 40 degrees of heel. This angle was taken as the critical downflooding angle, used in the calculation of the wind heeling lever itself.

In both cases, the intersection of the derived wind heeling curves and curves of statical stability occurs above the 15 degree lower limit specified, confirming that Boleh conforms to the requirements – approximately 23 degrees and 21 degrees for the 100% and 10% load cases respectively. The difference in draught between the two cases accounts for this change in intersection – for the 100% load case, the vessel sits slightly lower in the water and therefore experiences less of a heeling moment from the wind.

5.3 Results from CFD Mesh Dependency Analysis

Although the CFD investigation was incomplete, the mesh dependency analysis did provide some results of use. The analysis was performed for a single flow velocity, 0.8m/s. The initial mesh was intentionally coarse, with just over 300,000 cells. The mesh density was then increased incrementally using a scale factor within ICEM. Initially the increments were large, but as 1000,000 cells were reached, they were reduced in size. This was because the software licenses on the computers used limit the maximum number of cells to this value. It was therefore essential to capture as much detail as possible as the limit was approached, in order to make a prediction of behaviour with additional cells.

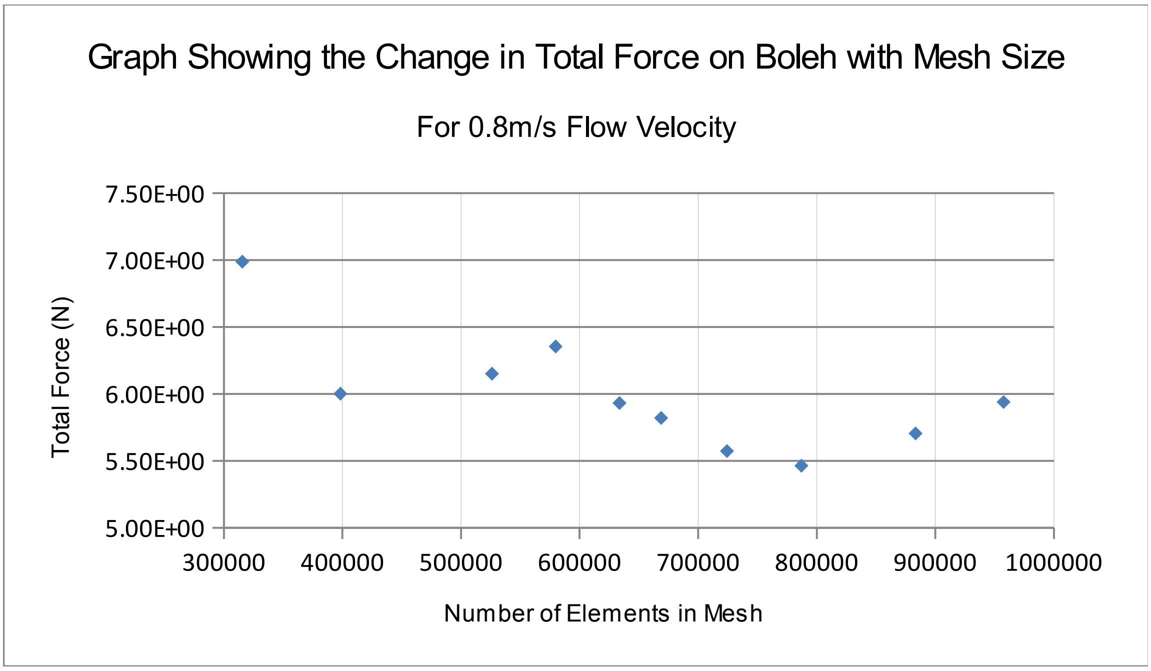

Figure 5.5: mesh dependency analysis results.

The graph 5.5 above illustrates the findings of the analysis. The first and most striking feature of the graph is the sinusoidal pattern of the curve – the forces are decreasing with mesh size, but are fluctuating as they do so. Secondly, the variations in force between the data points are not insignificant; in the towing tank testing, differences in force between runs were of a similar magnitude around the flow speed tested here. The variations are decreasing though as mesh size is increased, allowing for the irregular x-axis spacing of the points – observe the difference in force between the first and second points and the fifth and seventh, which are of similar spacing. Finally, the magnitude of the forces involved is several times higher than that found at the same speed in the towing tank testing. Full data from the mesh dependency analysis is available in appendix (X)

5.3.1 Discussion

These observations imply the following: that an ideally sized mesh has not yet been found, but is likely to be found as the trend is of decreasing force, and that despite this, the model needs further refinement due to the discrepancy in force between this test and the towing tank tests. Given the trend of the graph above , it seems unlikely that the forces will drop to a level close to that found from the tank tests.

Based on observations from the software set-up phase, the likely cause of the discrepancy in force is the turbulence length or intensity factor; this was based on a value from the CFX “bump” tutorial (Ansys, 2010), where it was erroneously specified at the same length/depth as the free surface. It was discovered later that the value controls the intensity of turbulence in the flow (Ansys, 2010); therefore it seems likely that the net turbulence was too energetic, resulting in too great a drag force on the vessel.

Once each run had been calculated, it was possible to use post processing software to visualise the simulated flow patterns. While no useful numerical results could be gathered from these visualisations, they did provide confirmation that the simulations, although in need of refinement, were successful. This first example demonstrates the effective simulation of the hydrostatic gradient:

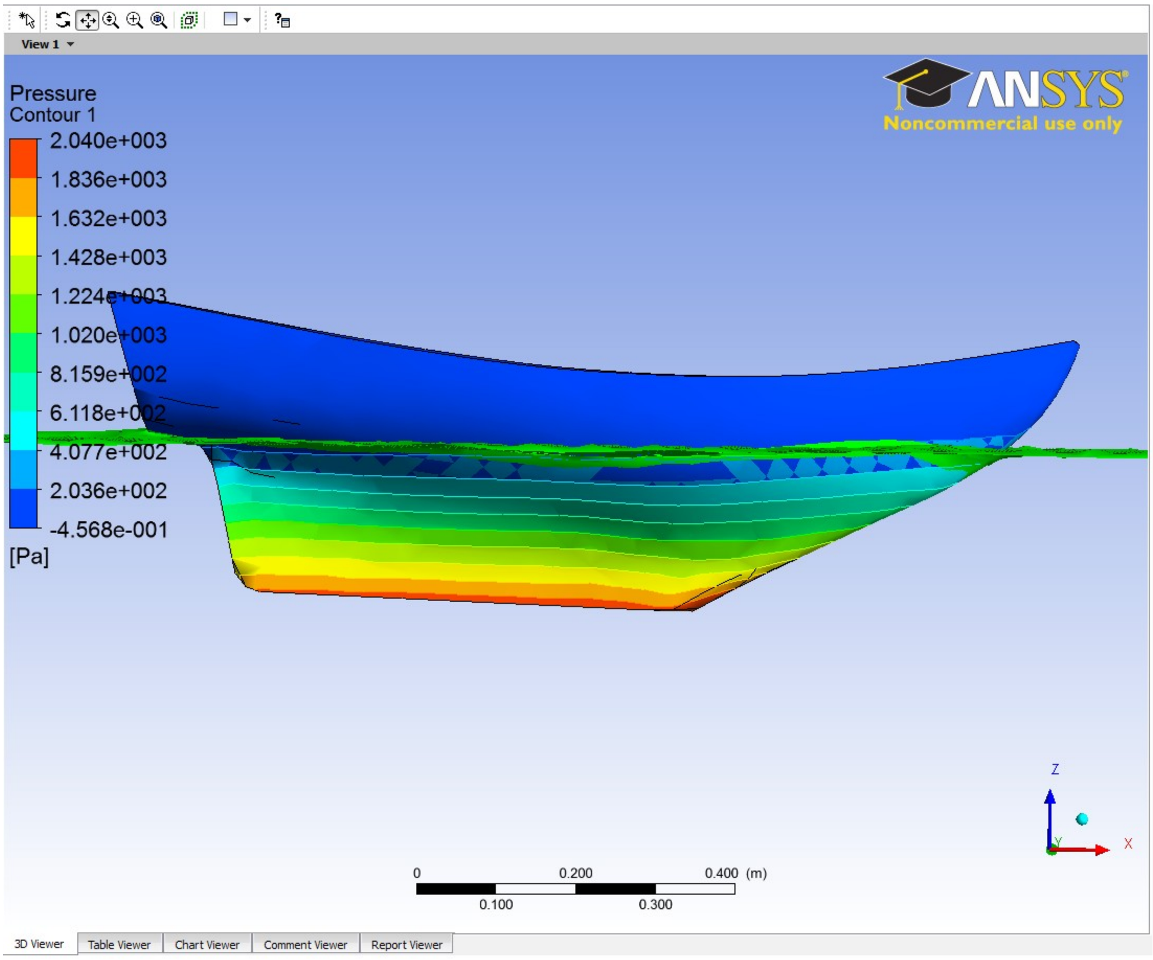

Figure 5.6: visualisation of the hydrostatic gradient for the mesh 10 of the 0.8m/s case. The light blue diamond shaped patches on the dark blue are a graphics error.

It can be seen in figure 5.6 that, as expected, the pressure increases linearly with depth. A quick hand calculation confirms the CFD calculated value of the highest pressure (shown on the left of the image), assuming an average draught of 0.206m. Note that the negative pressure shown at on the freeboard is due to the plotting of local rather than absolute pressure; atmospheric pressure was factored. Although the hydrostatic gradient is clearly visible, there is little evidence of the dynamic pressure; this is due to the magnitude of the pressures involved – at these relatively low speeds, the hydrostatic gradient is dominant. This is confirmed in the next example (see figure 5.7); for a single run, the speed was set artificially (7.5m/s) high in order to confirm that the flow was moving in the correct direction, and to help visualise the wave system:

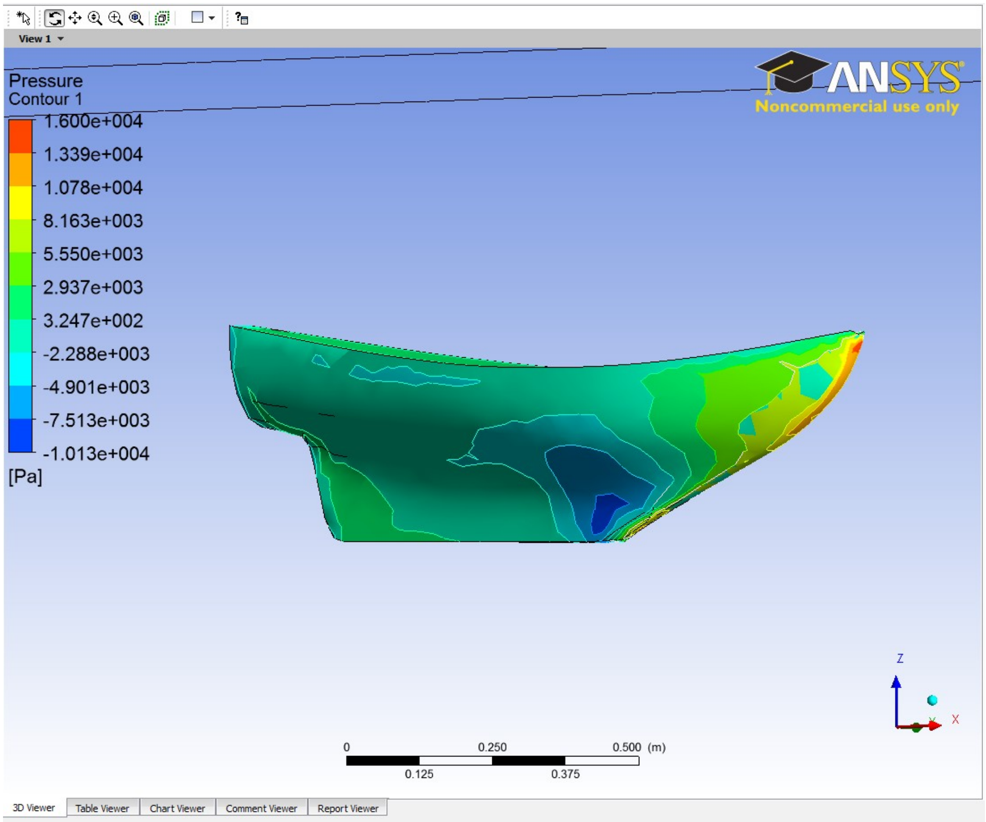

Figure 5.7: visualisation of the local pressure at 7.5m/s

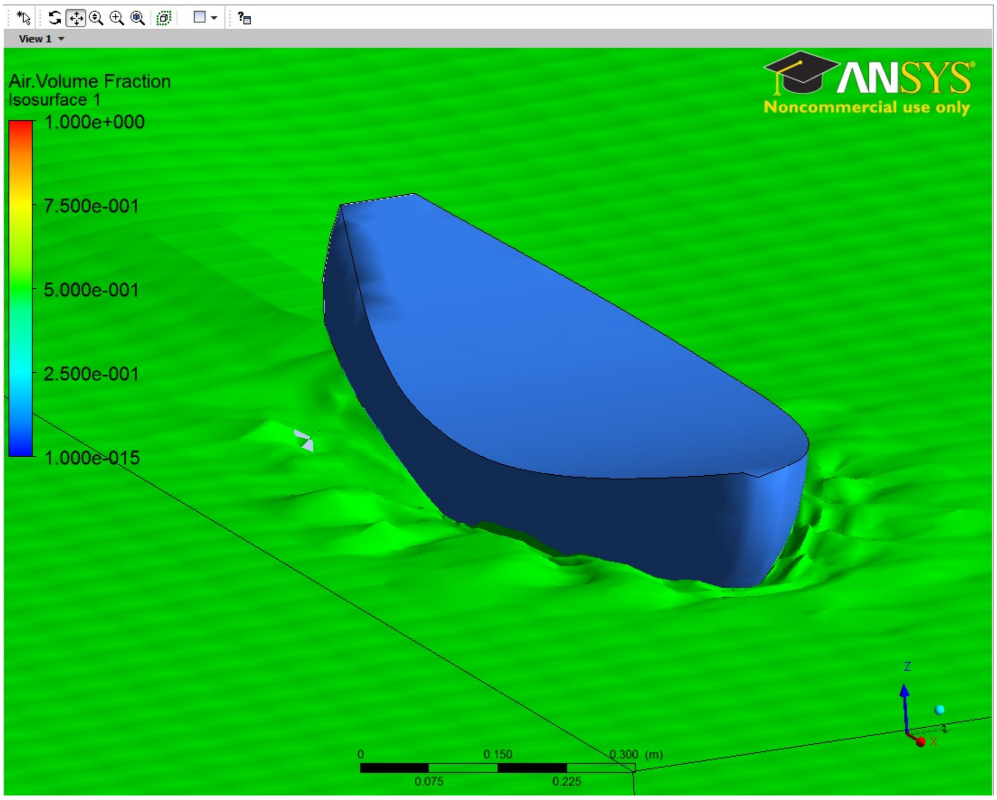

Figure 5.8: visualisation of the wave system at artificially (7.5m/s) high speed.

Figure 5.8 provides an excellent demonstration of the nature of the wave system generated by the simulation. It can be seen that even at this velocity, the waves are not radiating in the fashion observed in the towing tank. See figure (towing tank picture) for reference. The wake is visible as a barrel shaped hump behind the vessel.

Figure 5.6, which is taken directly from the side, does show that for the slower runs, the wave system immediately around the vessel conforms to the pattern observed. Aside from this detail, the expected radiation does not appear to be taking place at lower speeds either.

One possible explanation for the missing elements of the wave system is the coarseness of the mesh. The constant energy in each wave in the system causes the size of the waves to attenuate with distance from the hull (Rawson, K.J. and Tupper, E.C. 1996). The result of this in this context is that although the coarse mesh has the resolution to display the deeper ends of the waves adjacent to the hull, it struggles to draw them at greater distances – a higher resolution would be required. However, this will not affect the results as the pressure resistance which is responsible for the waves is defined over the surface of the vessel and not at a distance from it – in effect the correct conditions are being simulated, just not visualised.

6. Conclusions

To conclude the project as a whole, it can be said that although some parts of the experiments would benefit from further work, the project as a whole has been successful.

The CFD, although incomplete, showed great promise. The Mesh dependency analysis and observations from the post-processing demonstrated that although refinement was required, the basic methodology and simulation was sound. All of the physical phenomenon that were observed in the towing tank were replicated in some form or another in the CFD, and the results, although high compared to the towing tank tests, were falling in magnitude as the number of elements increased.

In regards to the tank tests, it was noted in the book by Commander Kilroy detailing *Boleh's* epic voyage that the 8hp motor used originally to propel *Boleh,* was capable of doing so at 4.5 knots in a flat calm (Kilroy R A, 1951). By comparison, the power derived from these tests in the same conditions is just over a tenth of this at the same speed (see appendix).

The empirical validation used does not really help the situation. Frictional forces dominate even up to the 4.5 knots under examination, and as both methods use the same ITTC formula to derive skin friction values, no conclusions can be drawn at this speed.

It seems invalid to draw too many conclusions for this without a more thorough power estimate than the naked hull prediction, as the estimate does not include appendage resistance, or explicitly account for hull roughness. Further, the original drive itself is noted as being temperamental, and its complicated shafting design is likely have to led to severe mechanical losses. On the other hand, the inaccuracy of the tank measurements at low speeds has been demonstrated with the negative power requirements of the calm, trim forwards case. This is doubtless due to the issues in measuring the very small forces produced at low speeds. Regardless of this, the powering estimates from the tank are too low – the disparity is too large to support any other argument.

The cause of the error is harder to determine. The results and scaling calculations were checked thoroughly for numerical errors in terms of order of magnitude, or properties at the tested tank temperatures. The friction inherent in the towing carriage and rails will not have had an effect on the magnitude of the results as the actual average speed of the run was measured, as compared to the speed set with the controls.

The remaining option is frictional resistance. The exact effect of the turbulence studs is unknown, as it was not possible to measure the turbulence around the vessel. If the flow was not sufficiently stimulated, the resistance of the model, and therefore the full vessel, would have been too low. Cf at the model scale would therefore have had too large an effect, by representing a flow type not measured and lowering the overall resistance by overly reducing Cr. Once Cr became more dominant at higher speeds, the effect was less severe and the results more accurate.

Regarding the stability assessment, *Boleh* is sufficiently stable, having passed the assessment criteria. Considering the vessel has sailed without major disaster from Singapore to England, this is unsurprising. Further, the margin between the minimal requirements and the derived values is sufficient that any error descending from the calculation of free surface effects should not prove dangerous in practice.

7. Future work

Although this project is complete, the work on restoring *Boleh* is still ongoing. This means that there is scope for future work of this nature on the vessel. For example, a full inclining experiment is required on the completed vessel upon her re-launch, which will provide an additional check on her stability before she returns to sea. Further, the computational stability assessment could be improved by a more thorough approach to the free surface problem - possibly by using a software package that allows greater control of the shape of the tanks and can therefore accurately model the effect.

The progress so far on the CFD is very promising and limited future work would be required to complete it. The issues of the force magnitudes must be addressed – it seems likely that the turbulence is too high for a flow of this velocity. Similarly, increasing the mesh density (the number of cells within the control volume) further would be necessary to complete the mesh dependency analysis, and eliminate mesh dependency as a factor. Once these points have been considered a full set of calm water resistance trials could be simulated and used for validation of the tank tests.

References

Kilroy R A, 1951, *Boleh*, Hodder and Stoughton, London.

Boleh Trust, 2013, *Boleh's History*. http://www.bolehproject.com/bolehs-history/. [Accessed 16/04/2013]

Happs, J, 2013. *An Analysis Of The Sailing Efficiency Of The Junk Yacht Boleh.* University of Southampton, Faculty of Engineering and the Environment.

Tan, M, 2011, *SESS2003 Resistance and Propulsion lecture notes.* University of Southampton, Faculty of Engineering and the Environment.

Rawson, K.J. and Tupper, E.C. 1996, *Basic Ship Theory Volume 2*, 4th ed. Oxford: Butterworth Heinemann

Comstock, J P (editor), 1967. *Principals of Naval Architecture*. New York: The Society of Naval Architects and Marine Engineers.

International Towing Tank Conference, 1999, *ITTC Recommended Procedures, Performance, Propulsion 1978 ITTC Performance Prediction Method* [PDF]. Available at: <http://ittc.sname.org/2006_recomm_proc/7.5-02-03-01.4.pdf>[Accessed 16/04/2013]

Molland A F, 2002, *SESS3006 Marine Propulsion Engineering lecture notes*. University of Southampton, Faculty of Engineering and the Environment.

International Towing Tank Conference, 2006, *ITTC Recommended Procedures and Guidelines, Testing and Extrapolation Methods,* General Density and Viscosity of Water [PDF]. Available at: <http://ittc.sname.org/2006_recomm_proc/7.5-02-01-03.pdf>[Accessed 16/04/2013]

International Towing Tank Conference, 2002, *ITTC recommended Procedures and Guidelines, Model Manufacture, Ship Models* [PDF]. Available at: <http://ittc.sname.org/2006_recomm_proc/7.5-01-01-01.pdf>[Accessed 03/12/2012]

Robert, F., Pritchard, P. and McDonald, A, 2010, *Introduction to Fluid Mechanics,* 7th ed. Asia: Wiley.

Gemba, K, 2007, *Measurement of Boundary Layer on a Flat Plate,* California State University, Long beach. [PDF]. Available at: <http://kai.gemba.org/pdf/MAE440/MAE440Exp03.pdf>.
[Accessed 03/12/2012]

Rawson, K.J. and Tupper, E.C.,2001, *Basic Ship Theory Volume 1*, 5th ed. Oxford: Butterworth Heinemann

Versteeg H K and Malalasekera, 1995, *An Introduction to Computational Fluid Dynamics: The Finite Volume Method*. Longman Scientific and Technical, Harlow.
ISBN 0-582-21884-5

Shaw C T, 1992, *Using Computational Fluid Dynamics.* Prentice hall, Hemel Hempstead.
ISBN 0-13-928714-0

Anderson, J, 1995, *Computational Fluid Dynamics, The Basics With Applications.* New York: McGraw-Hill Science.

Mohd ARIFF, Salim M. SALIM* and Siew Cheong, 2009, *Cheah, Wall Y+ Approach For Dealing With Turbulent Flow Over A Surface Mounted Cube: Part 2 – High Reynolds Number*[PDF]. Available at:<http://www.cfd.com.au/cfd_conf09/PDFs/142SAL.pdf> [Accessed 03/12/2012]

Salim S M and Cheah S C, 2009. *Wall y+ Strategy for Dealing with Wall-bounded Turbulent Flows.* In: Proceedings of the International MultiConference of Engineers and Computer Scientists 2009 Vol II IMECS 2009, March 18 - 20, 2009, Hong Kong.
ISBN: 978-988-17012-7-5

Gerritsma, Beukelman, 1972, *Analysis of the Resistance Increase in Waves of a Fast Cargo Ship,* In: International Shipbuilding Progress, Volume 19.

Hogben N, Dacunha N M C and Oliver G F, 1986. *Global Wave Statistics.* British Maritime Technology Limited, Feltham. ISBN 0 946653 38 0

Maritime and Coastguard Agency, 2004, *MGN280 (M) Small Vessels in Commercial Use for Sport or Pleasure, Workboats and Pilot Boats – Alternative Construction Standards.* [PDF]. Available at:
<http://www.dft.gov.uk/mca/mgn_280-2.pdf>[Accessed 03/12/2012]

Calvert J R and Farrar R A, 2008. *An Engineering Data Book.* Palgrave Macmillan, Basingstoke. ISBN-13: 978-0-230-22033-1

Fossati, F, 2009, *Aero-Hydrodynamics and the Performance of Sailing Yachts.* London, Adlard Coles Nautical. ISBN 978-1-4081-1338-7

Xie Z, 2012. *SESS6021 lab3 (Week 3) for Fluent groups*. University of Southampton. Faculty of Engineering and the Environment.

Wilson P A, 2012. *SESS3001 Marine Hydrodynamics lecture notes.* University of Southampton. Faculty of Engineering and the Environment.

Ansys, 2010. *Ansys CFX Tutorials:Chapter 9: Free Surface Flow over a Bump.* [PDF] Available at:
<https://support.ansys.com/portal/site/AnsysCustomerPortal/searchnav?keyword=cfx>.[Accessed 16/04/2013]

Holtrop J and Mennen G G J, 1982. *An approximate Power Prediction Method.* [PDF] Available at <http://esrdc.mit.edu/library/ESRDC_library/Holtrop-Approximate-1982.pdf>[Accessed 16/04/20123]

Appendix 1 – Particulars of *Boleh*

The figures presented here represent *Boleh's* characteristics. They describe Boleh fully laden (unless stated otherwise) at her design waterline, with values for centres of gravity for the sails up position. The datum is the design waterline-midships-centreline intersection. These values were the ones used during the project, and were largely determined from the Maxsurf model described above. The KG values include the effects of the free surface.

Displacement (100% loaded)	18.31	t
Displacement (10% loaded)	17.85	t
Draft Amidships (100% loaded)	2.06	m
Draft Amidships (10% loaded)	2.04	m
WL Length	10.245	m
Beam max extents on WL	3.432	m
Wetted Area	45.957	m^2
Max sect. area	3.273	m^2
Waterpl. Area	24.831	m^2
Prismatic coeff. (Cp)	0.533	
Block coeff. (Cb)	0.248	
Max Sect. area coeff. (Cm)	0.466	
Waterpl. area coeff. (Cwp)	0.706	
LCB length	0.307	'frd (m)
LCF length	0.155	'frd (m)
Immersion (TPc)	0.255	tonne/cm
MTc	0.135	tonne.m
Length:Beam ratio	2.985	
Beam:Draft ratio	1.675	
Length:Vol^0.333 ratio	3.919	
Vertical Centre of Gravity (100% loaded) inc. FS	-0.577	m
Vertical Centre of Gravity (10% loaded) inc. FS	-0.873	m

Table A.1.1: particulars of *Boleh*

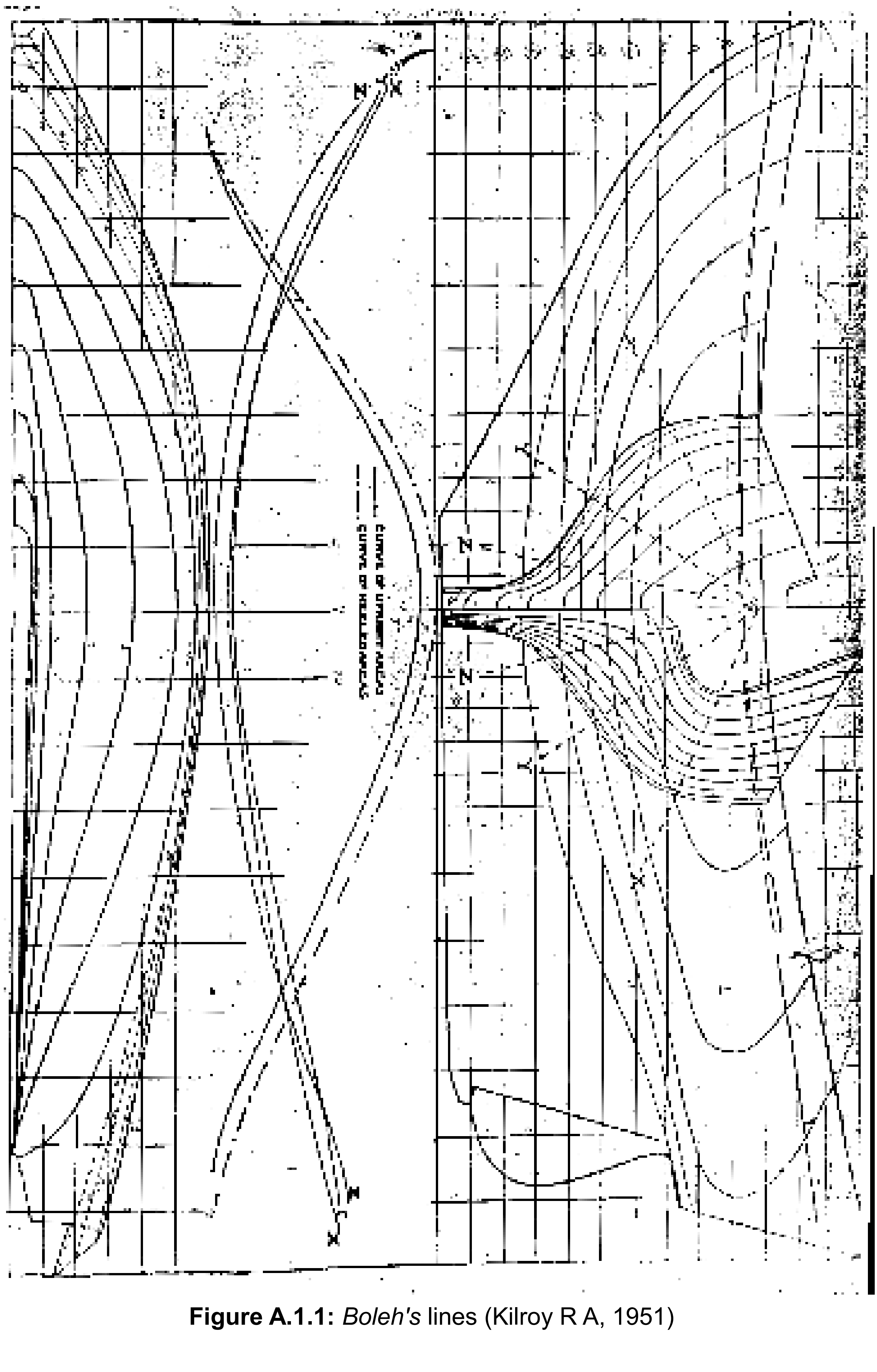

Figure A.1.1: *Boleh's* lines (Kilroy R A, 1951)

Figure A.1.2: *Boleh* under sail (Boleh trust, 2013)

Appendix 2 – Data

The data presented here is the processed data from the towing tank and CFD experiments, and the stability assessment. The raw data has not been included from the CFD or towing tank dynamometer – the quantity was too far great for this to be considered.

A.2.1 Towing tank test results

The results from the towing tank tests are shown here based on water and trim conditions. Values shown are averages, either from the dynamometer values or from runs and re-runs. The temperature corrected values are all at ship scale. All values used in the derivation of the Reynolds numbers (and therefore Cf values) are from the ITTC paper (2006) or derived from the particulars above.

Calm, no trim

Ship speed (knots)	Ship speed (m/s)	Model speed (m/s)	Re (model)	Re (ship)	Drag (model)	Cf Model	Cf ship	Ct Model	Cr (Shared)	Ct Ship	Re (15 degrees)	Cf(15 degrees)	Corrected Ct (15 degrees)	Drag ship (N)	Power (kW)
2.03	1.04	0.33	2.66E+005	8.42E+06	0.208	0.006392	0.003092	0.00831	0.00191	0.00501	8.99E+006	0.00306	0.00497	127.6	0.133
3.26	1.68	0.53	4.28E+005	1.35E+07	0.414	0.005688	0.002849	0.00641	0.00072	0.00357	1.44E+007	0.00282	0.00354	234.4	0.393
4.49	2.31	0.73	5.89E+005	1.86E+07	0.594	0.005277	0.002700	0.00485	-0.00042	0.00228	1.99E+007	0.00267	0.00225	282.5	0.652
4.92	2.53	0.8	6.46E+005	2.04E+07	0.888	0.005167	0.002660	0.00604	0.00087	0.00353	2.18E+007	0.00263	0.00351	528.9	1.338
6.33	3.26	1.03	8.31E+005	2.63E+07	1.526	0.004882	0.002553	0.00626	0.00138	0.00393	2.81E+007	0.00253	0.00391	977.3	3.183
6.95	3.57	1.13	9.12E+005	2.88E+07	1.916	0.004783	0.002516	0.00653	0.00175	0.00427	3.08E+007	0.00249	0.00424	1276.8	4.562
8.18	4.21	1.33	1.07E+006	3.39E+07	3.576	0.004616	0.002452	0.00880	0.00419	0.00664	3.62E+007	0.00243	0.00661	2757.5	11.598
9.22	4.74	1.5	1.21E+006	3.83E+07	7.169	0.004499	0.002406	0.01387	0.00937	0.01178	4.09E+007	0.00238	0.01175	6235.6	29.578

Calm, trim aft

Ship speed (knots)	Ship speed (m/s)	Model speed (m/s)	Re (model)	Re (ship)	Drag (model)	Cf Model	Cf ship	Ct Model	Cr (Shared)	Ct Ship	Re (15 degrees)	Cf(15 degrees)	Corrected Ct (15 degrees)	Drag ship (N)	Power (kW)
2.03	1.04	0.33	2.66E+005	8.42E+06	0.098	0.006393	0.003092	0.00393	-0.00247	0.00062	8.99E+006	0.00306	0.00059	15.1	0.016
3.26	1.68	0.53	4.27E+005	1.35E+07	0.485	0.005689	0.002849	0.00751	0.00182	0.00467	1.44E+007	0.00282	0.00464	307.4	0.515
4.49	2.31	0.73	5.89E+005	1.86E+07	0.811	0.005277	0.002701	0.00663	0.00135	0.00405	1.99E+007	0.00267	0.00402	505.0	1.166
5.10	2.62	0.83	6.69E+005	2.12E+07	0.927	0.005124	0.002644	0.00586	0.00073	0.00338	2.26E+007	0.00262	0.00335	543.7	1.427
6.33	3.26	1.03	8.31E+005	2.63E+07	1.742	0.004882	0.002554	0.00715	0.00227	0.00482	2.80E+007	0.00253	0.00479	1198.7	3.904
6.95	3.57	1.13	9.11E+005	2.88E+07	2.057	0.004783	0.002516	0.00701	0.00223	0.00475	3.08E+007	0.00249	0.00472	1420.7	5.077
8.18	4.21	1.33	1.07E+006	3.39E+07	3.503	0.004617	0.002452	0.00862	0.00401	0.00646	3.62E+007	0.00243	0.00643	2682.8	11.283
9.41	4.84	1.53	1.23E+006	3.90E+07	6.807	0.004481	0.002399	0.01266	0.00818	0.01058	4.17E+007	0.00237	0.01055	5824.2	28.179

Calm, trim forwards

Ship speed (knots)	Ship speed (m/s)	Model speed (m/s)	Re (model)	Re (ship)	Drag (model)	Cf Model	Cf ship	Ct Model	Cr (Shared)	Ct Ship	Re (15 degrees)	Cf(15 degrees)	Corrected Ct (15 degrees)	Drag ship (N)	Power (kW)
2.03	1.04	0.33	2.51E+005	3.08E-02	0.031	0.006487	0.003123	0.00123	-0.00526	-0.00213	8.99E+006	0.00306	-0.00220	-56.5	-0.059
3.26	1.68	0.53	4.04E+005	2.52E-01	0.252	0.005768	0.002818	0.00390	-0.00186	0.00095	1.44E+007	0.00282	0.00095	63.1	0.106
4.49	2.31	0.73	5.56E+005	5.64E-01	0.564	0.005348	0.002672	0.00460	-0.00074	0.00193	1.99E+007	0.00267	0.00193	242.2	0.559
5.10	2.62	0.83	6.32E+005	7.14E-01	0.714	0.005192	0.002616	0.00451	-0.00068	0.00194	2.26E+007	0.00262	0.00194	314.9	0.826
6.33	3.26	1.03	7.84E+005	1.32E+00	1.316	0.004945	0.002527	0.00540	0.00045	0.00298	2.80E+007	0.00253	0.00298	745.7	2.429
6.95	3.57	1.13	8.61E+005	1.81E+00	1.805	0.004844	0.002490	0.00615	0.00131	0.00380	3.08E+007	0.00249	0.00380	1143.7	4.087
8.05	4.14	1.31	9.98E+005	3.70E+00	3.695	0.004690	0.002433	0.00937	0.00468	0.00712	3.57E+007	0.00243	0.00712	2878.8	11.926
9.41	4.84	1.53	1.17E+006	7.50E+00	7.502	0.004536	0.002375	0.01395	0.00941	0.01179	4.17E+007	0.00237	0.01179	6505.8	31.477

Table A.2.1: results for calm water conditions

Modcratc, no trim

Ship speed (knots)	Ship speed (m/s)	Model speed (m/s)	Re (model)	Re (ship)	Drag (model)	Cf Model	Cf ship	Ct Model	Cr (Shared)	Ct Ship	Re (15 degrees)	Cf(15 degrees)	Corrected Ct (15 degrees)	Drag ship (N)	Power (kW)
2.09	1.08	0.34	2.52E+005	7.95E+06	0.497	0.006486	0.003123	0.01872	0.01224	0.01536	9.26E+006	0.00304	0.01528	416.3	0.448
3.26	1.68	0.53	3.92E+005	1.24E+07	0.565	0.005808	0.002891	0.00876	0.00295	0.00584	1.44E+007	0.00282	0.00577	381.9	0.640
4.30	2.21	0.7	5.18E+005	1.64E+07	0.645	0.005437	0.002759	0.00573	0.00030	0.00306	1.91E+007	0.00269	0.00299	345.1	0.764
4.92	2.53	0.8	5.92E+005	1.87E+07	0.864	0.005271	0.002698	0.00588	0.00061	0.00331	2.18E+007	0.00263	0.00324	488.8	1.237
6.27	3.23	1.02	7.55E+005	2.39E+07	1.460	0.004988	0.002593	0.00611	0.00112	0.00371	2.78E+007	0.00253	0.00365	895.6	2.889
6.95	3.57	1.13	8.36E+005	2.64E+07	2.110	0.004875	0.002551	0.00719	0.00232	0.00487	3.08E+007	0.00249	0.00481	1446.6	5.169
8.18	4.21	1.33	9.84E+005	3.11E+07	3.414	0.004704	0.002486	0.00840	0.00370	0.00618	3.62E+007	0.00243	0.00612	2554.0	10.742
9.41	4.84	1.53	1.13E+006	3.58E+07	7.338	0.004564	0.002432	0.01364	0.00908	0.01151	4.17E+007	0.00237	0.01145	6321.6	30.585

Moderate, trim aft

Ship speed (knots)	Ship speed (m/s)	Model speed (m/s)	Re (model)	Re (ship)	Drag (model)	Cf Model	Cf ship	Ct Model	Cr (Shared)	Ct Ship	Re (15 degrees)	Cf(15 degrees)	Corrected Ct (15 degrees)	Drag ship (N)	Power (kW)
2.09	1.08	0.34	2.51E+005	7.95E+06	0.303	0.006487	0.003123	0.01140	0.00492	0.00804	9.26E+006	0.00304	0.00796	216.9	0.233
3.26	1.68	0.53	3.92E+005	1.24E+07	0.513	0.005809	0.002891	0.00795	0.00214	0.00503	1.44E+007	0.00282	0.00495	328.1	0.550
4.49	2.31	0.73	5.40E+005	1.71E+07	0.808	0.005384	0.002740	0.00660	0.00122	0.00396	1.99E+007	0.00267	0.00389	488.6	1.128
4.92	2.53	0.8	5.92E+005	1.87E+07	0.891	0.005271	0.002698	0.00606	0.00079	0.00349	2.18E+007	0.00263	0.00342	515.8	1.305
6.33	3.26	1.03	7.62E+005	2.41E+07	1.895	0.004978	0.002590	0.00777	0.00280	0.00539	2.80E+007	0.00253	0.00532	1331.5	4.337
6.76	3.48	1.1	8.13E+005	2.57E+07	2.446	0.004905	0.002562	0.00880	0.00389	0.00646	3.00E+007	0.00250	0.00639	1824.1	6.345
8.18	4.21	1.33	9.83E+005	3.11E+07	4.512	0.004705	0.002486	0.01110	0.00640	0.00888	3.62E+007	0.00243	0.00882	3680.0	15.477
9.41	4.84	1.53	1.13E+006	3.58E+07	10.770	0.004564	0.002432	0.02002	0.01546	0.01789	4.17E+007	0.00237	0.01784	9843.3	47.625

Empirical Estimate

V knots	Speed (m/s)	Rn (15)	Cf(15)	Rf (N)	Rw(N)	Ra	Total resistance (N)	Power (KW)
2.02	1.04	8.99E+006	0.003056	78.5	0.0	19.90244	130.11	0.14
3.25	1.68	1.44E+007	0.002817	186.6	0.4	51.33695	313.78	0.53
4.48	2.31	1.99E+007	0.002671	335.6	27.1	97.39218	595.92	1.38
4.91	2.53	2.18E+007	0.002632	397.1	82.5	116.9656	757.18	1.92
6.32	3.26	2.81E+007	0.002527	632.0	731.9	193.8888	1813.38	5.91
6.93	3.57	3.08E+007	0.002490	749.6	1632.5	233.3647	2918.62	10.43
8.16	4.21	3.62E+007	0.002427	1012.1	7415.1	323.2821	9159.88	38.52
9.20	4.74	4.09E+007	0.002382	1263.5	17660.6	411.2074	19846.36	94.14

Table A.2.2: results for moderate conditions and empirical estimate.

A.2.2 Results from stability assessment

Heel Angle degrees	Righting GZ metres	Trim metres	VCB metres	GZ Curve Area metres.rad	Derived Wind Lever (m)
0	0	0	-0.555	0	0.4023019279
5	0.083	-0.005	-0.551	0.004	0.4003129205
10	0.165	-0.017	-0.541	0.015	0.3943746676
15	0.244	-0.036	-0.524	0.032	0.3845732083
20	0.318	-0.057	-0.501	0.057	0.3710510589
25	0.389	-0.078	-0.472	0.088	0.3540059315
30	0.456	-0.097	-0.438	0.125	0.3336890344
35	0.518	-0.115	-0.399	0.167	0.3104030567
40	0.569	-0.135	-0.359	0.215	0.2845
45	0.612	-0.156	-0.317	0.266	0.2563790991
50	0.646	-0.179	-0.275	0.321	0.226485217
55	0.673	-0.199	-0.23	0.379	0.1953083479
60	0.696	-0.214	-0.182	0.439	0.163385353
65	0.717	-0.223	-0.13	0.5	0.131306085
70	0.737	-0.222	-0.07	0.564	0.0997285044
75	0.764	-0.2	0.004	0.629	0.0694140232
80	0.799	-0.135	0.093	0.697	0.0413164899
85	0.817	-0.073	0.172	0.768	0.0168630814
90	0.813	-0.039	0.236	0.839	1.71713E-012
95	0.779	-0.013	0.276	0.909	-
100	0.731	0.014	0.308	0.975	-
105	0.675	0.04	0.338	1.036	-
110	0.613	0.065	0.365	1.092	-
115	0.546	0.089	0.391	1.143	-
120	0.476	0.105	0.418	1.188	-
125	0.406	0.111	0.447	1.226	-
130	0.338	0.107	0.477	1.259	-
135	0.271	0.095	0.508	1.285	-
140	0.207	0.08	0.54	1.306	-
145	0.148	0.063	0.572	1.321	-
150	0.096	0.046	0.606	1.332	-
155	0.054	0.032	0.639	1.339	-
160	0.026	0.024	0.672	1.342	-
165	0.015	0.024	0.703	1.344	-
170	0.009	0.028	0.727	1.345	-
175	0.004	0.031	0.742	1.345	-
180	0	0.032	0.746	0	-

Table A.2.3: 100% load condition GZ and wind heeling lever values inc. free surface effects.

Heel Angle degrees	Righting GZ metres	Trim metres	VCB metres	GZ Curve Area metres.rad	Derived Wind Lever (m)
0	0	0	-0.569	0	0.4936023354
5	0.115	-0.004	-0.565	0.005	0.4911619328
10	0.229	-0.016	-0.555	0.02	0.483876023
15	0.339	-0.034	-0.538	0.045	0.4718501717
20	0.444	-0.054	-0.515	0.079	0.4552592382
25	0.544	-0.075	-0.486	0.122	0.4343458046
30	0.64	-0.093	-0.451	0.174	0.4094180894
35	0.73	-0.11	-0.411	0.234	0.3808474757
40	0.809	-0.129	-0.37	0.301	0.34906585
45	0.876	-0.149	-0.327	0.375	0.3145630515
50	0.934	-0.171	-0.283	0.454	0.2778849026
55	0.983	-0.19	-0.237	0.537	0.2396325993
60	1.025	-0.204	-0.187	0.625	0.2004648404
65	1.062	-0.213	-0.132	0.716	0.1611053433
70	1.098	-0.211	-0.069	0.81	0.1223613889
75	1.14	-0.191	0.01	0.908	0.0851671881
80	1.184	-0.132	0.102	1.009	0.0506930603
85	1.206	-0.08	0.182	1.114	0.0206900732
90	1.199	-0.052	0.243	1.219	2.10682E-012
95	1.161	-0.028	0.282	1.322	-
100	1.107	-0.004	0.314	1.421	-
105	1.043	0.02	0.343	1.515	-
110	0.969	0.044	0.37	1.603	-
115	0.887	0.068	0.396	1.684	-
120	0.801	0.086	0.423	1.758	-
125	0.712	0.094	0.451	1.824	-
130	0.622	0.093	0.481	1.882	-
135	0.532	0.084	0.512	1.932	-
140	0.442	0.07	0.545	1.975	-
145	0.357	0.054	0.577	2.009	-
150	0.277	0.039	0.611	2.037	-
155	0.205	0.026	0.645	2.058	-
160	0.147	0.019	0.679	2.073	-
165	0.105	0.019	0.71	2.084	-
170	0.07	0.023	0.735	2.092	-
175	0.035	0.027	0.75	2.096	-
180	0	0.029	0.755	0	-

Table A.2.4: 10% load condition GZ and wind heeling lever values inc. free surface effects.

A.2.3 Results from CFD analysis

The results from the mesh dependency analysis are presented here. Note that the forces are listed as negative because they are calculated as being opposite to the flow direction.

Run	Elements	Viscous force on hull (N)	Pressure force on hull (N)	Total force on hull (N)	Iterations to convergence	convergence time (mins)	mesh scale factor
1	315464	-9.47E-01	-6.04E+00	6.99E+00	89.00	28:05:00	1.200
2	398229	-9.07E-01	-5.10E+00	6.00E+00	113.00	43:21:00	1.100
3	526012	-8.42E-01	-5.31E+00	6.15E+00	86.00	43:39:00	1.000
4	579741	-8.89E-01	-5.47E+00	6.35E+00	91.00	51:28:00	0.975
5	633555	-9.01E-01	-5.03E+00	5.93E+00	97.00	61:41:00	0.950
6	668650	-8.61E-01	-4.96E+00	5.82E+00	98.00	62:32:00	0.925
7	724304	-8.31E-01	-4.74E+00	5.57E+00	99.00	68:17:00	0.900
8	787079	-8.36E-01	-4.63E+00	5.46E+00	115.00	87:35:00	0.875
9	883396	-8.37E-01	-4.87E+00	5.70E+00	83.00	70:50:00	0.850
10	957635	-8.58E-01	-5.08E+00	5.94E+00	90.00	85:30:00	0.825

Table A.2.5: mesh dependency analysis results.